Wilfrid Laurier University

Scholars Commons @ Laurier

Theses and Dissertations (Comprehensive)

2009

# Applications of New Diffusion Models to Barrier Option Pricing and First Hitting Time in Finance

Keang Ly
*Wilfrid Laurier University*

Follow this and additional works at: https://scholars.wlu.ca/etd

Part of the Mathematics Commons

## Recommended Citation

Ly, Keang, "Applications of New Diffusion Models to Barrier Option Pricing and First Hitting Time in Finance" (2009). *Theses and Dissertations (Comprehensive)*. 916.
https://scholars.wlu.ca/etd/916

This Thesis is brought to you for free and open access by Scholars Commons @ Laurier. It has been accepted for inclusion in Theses and Dissertations (Comprehensive) by an authorized administrator of Scholars Commons @ Laurier. For more information, please contact scholarscommons@wlu.ca.

Library and
Archives Canada

Published Heritage
Branch

395 Wellington Street
Ottawa ON K1A 0N4
Canada

Bibliothèque et
Archives Canada

Direction du
Patrimoine de l'édition

395, rue Wellington
Ottawa ON K1A 0N4
Canada

*Your file Votre référence*
*ISBN: 978-0-494-49985-6*
*Our file Notre référence*
*ISBN: 978-0-494-49985-6*

NOTICE:
The author has granted a non-exclusive license allowing Library and Archives Canada to reproduce, publish, archive, preserve, conserve, communicate to the public by telecommunication or on the Internet, loan, distribute and sell theses worldwide, for commercial or non-commercial purposes, in microform, paper, electronic and/or any other formats.

The author retains copyright ownership and moral rights in this thesis. Neither the thesis nor substantial extracts from it may be printed or otherwise reproduced without the author's permission.

AVIS:
L'auteur a accordé une licence non exclusive permettant à la Bibliothèque et Archives Canada de reproduire, publier, archiver, sauvegarder, conserver, transmettre au public par télécommunication ou par l'Internet, prêter, distribuer et vendre des thèses partout dans le monde, à des fins commerciales ou autres, sur support microforme, papier, électronique et/ou autres formats.

L'auteur conserve la propriété du droit d'auteur et des droits moraux qui protège cette thèse. Ni la thèse ni des extraits substantiels de celle-ci ne doivent être imprimés ou autrement reproduits sans son autorisation.

---

In compliance with the Canadian Privacy Act some supporting forms may have been removed from this thesis.

While these forms may be included in the document page count, their removal does not represent any loss of content from the thesis.

Conformément à la loi canadienne sur la protection de la vie privée, quelques formulaires secondaires ont été enlevés de cette thèse.

Bien que ces formulaires aient inclus dans la pagination, il n'y aura aucun contenu manquant.

Canada

# Applications of New Diffusion Models to Barrier Option Pricing and First Hitting Time in Finance

Keang Ly

B.Sc., Wilfrid Laurier University, 2006

THESIS

Submitted to the Department of Mathematics in partial fulfilment of
the requirements for Master of Science in Mathematics
Wilfrid Laurier University

©Keang Ly
Wilfrid Laurier University

2009

# *Acknowledgement*

A journey is easier when you travel together. Interdependence is certainly more valuable than independence. This thesis is the result of one and half years of work whereby I have been accompanied and supported by many people. I, Keang Ly, would like to express my appreciation to all those who have helped and given me the possibility to complete this master's thesis.

I want to thank the mathematics department at Wilfrid Laurier for providing me the office and tools that made it much more convenient and effective for my study and research.

It is difficult to overstate my sincere gratitude to my M.Sc. supervisor, Dr. Joe Campolieti from Wilfrid Laurier University who has guided me through this master's thesis. With his enthusiasm, inspiration, and great efforts, he has undoubtedly explained the concepts of financial mathematics. Throughout my thesis writing, he granted the support, expressed advice, provided excellent teaching, good company and plenty of ideas. I would not be accomplished without him.

I am indebted to many professors, Dr. Cristina Stoica, Dr. Anthony Bonato, Dr. Syd Bulman-Fleming and Dr. David Vaughan, who have assisted me to be accepted in this master program. In particular, I am grateful to Dr. Roman Markarov and Dr. Y. George Lai for their thoughtfulness of helping me with random questions that I struggled with. I also thank the committee who is valuating this master's thesis.

Finally, I would like to thank my family for their support with all financial assistance and encouragement and all my friends with whom I hung out and and studied with.

# *Abstract*

The main focus of this thesis is in the application of a new family of analytical solvable diffusion models to arbitrage-free pricing exotic financial derivatives, such as barrier options. The family of diffusions is the so-called "Drifted Bessel family" having nonlinear (smile-like) local volatility with multiple adjustable parameters. In particular, the drifted Bessel-$K$ diffusion is used to model asset (stock) price processes under a risk-neutral measure whereby discounted asset price are martingales.

Closed-form spectral expansions for barrier option values are derived within the Bessel-$K$ family of models. This follow from the closed-form spectral expansions for the transition probability densities which are obtained for the Bessel family of processes with imposed killing boundaries. We also show that the commonly adopted CEV model is recovered as a special parametric limit of our Bessel family of models for the case of zero drift.

The rapid convergence of the spectral expansions leads to very efficient numerical implementations of barrier option pricing and sensitivity analysis. We hence carry out various numerical computations in order to study the relative effects of the parameters (state dependencies) of the Bessel family of models with respect to barrier option pricing and hedging. We compare our results with the standard Black-Scholes (GBM) and CEV models, demonstrating that model specification leads to important differences when pricing non-vanilla options, such as barrier options.

# Contents

List of Figures v

Introduction 1

Chapter 1. Spectral Expansion For Underlying Processes 5

1.1. Transition Density and Fundamental Solutions 5

1.2. Squared Bessel Process 10

Chapter 2. Spectral Expansions for Transformed F-Diffusions 15

2.1. Canonical Transformation Methodology 15

2.2. First Hitting Time 18

2.3. Drifted Bessel Family of F-Diffusions 21

2.4. Transition Density for Drifted Bessel-$K$ Family 24

Chapter 3. Pricing Formulas For F-Diffusions 29

3.1. European Barrier Call Options 39

3.2. European Barrier Put Options 51

3.3. Recovering CEV Models from Bessel K-Subfamily 62

Chapter 4. Sensitivity Analysis For European Barrier Call Option 75

4.1. Delta 76

4.2. Theta 78

Conclusion and Future Work 81

Bibliography 85

# List of Figures


2.2.1 Typical paths depicting first hitting times. 21

2.3.1 Typical local volatility curves for the Bessel $K$-subfamily. 23

2.3.2 Typical local volatility curves for the Bessel $I$-subfamily. 24

2.4.1 Rapid convergence of series in (2.4.1). 25

2.4.2 Converged p.d.f.s. 26

3.0.1 Typical double barrier payoff ( note $t = T$). 31

3.0.2 Rapid convergence of c.d.f.s. 35

3.0.3 converged c.d.f.s. 35

3.0.4 Rapid convergence of related c.d.f.s. 38

3.0.5 Converged related c.d.fs. 38

3.1.1 Rapid convergence of double knock-out call series expansion. 40

3.1.2 Converged double knock-out call. 41

3.1.3 Converged double knock-out call option value. 42

3.1.4 Converged double knock-out call value. 43

3.1.5 Convergence of spectral expansion for double knock-out call. 44

3.1.6 Converged double knock-out call value where $K < L < H$. 45

3.1.7 Converged double knock-out call value. 45

3.1.8 Converged double knock-out call values with $K < L < H$. 46

3.1.9 Convergence of down-and-out call value. 47

3.1.10 Converged down-and-out call in comparison with GBM model. 48

3.1.11 Convergence of double knock-out call to the up-and-out call. 50

3.1.12 Converged up-and-out call in comparison with GBM model. 50

3.2.1 Rapid convergence of the spectral expansion for equation (3.2.3). 53

3.2.2 Converged double knock-out put values with various $K$ values. 54

3.2.3 Converged double knock-out put value with various $T$. 54

3.2.4 Converged double Knock-Out put for three sets of $(\mu, a)$. 55

3.2.5 Series convergence for double knock-out put with $L \leq H \leq K$. 56

3.2.6 Converged double knock-out put option value for various $K$. 57

3.2.7 Converged double knock-out put values with various $T$. 57

3.2.8 Converged double knock-out put with different choices of $(\mu, a)$. 58

3.2.9 Convergence of up-and-out put value. 61

3.2.10 Converged up-and-out put value and GBM model. 61

3.3.1 Convergence of CEV transition density. 65

3.3.2 Converged CEV density with various $t$. 65

3.3.3 Convergence of double knock-out call series for CEV model. 68

3.3.4 Converged double knock-out European call value CEV model. 68

3.3.5 Converged double-knock-out CEV model with various maturities. 69

3.3.6 double knock-out call CEV model with $K \leq L \leq H$. 70

3.3.7 Double-knock-out call for CEV model with various $T$ values. 70

3.3.8 Rapidly convergent double-knock-out put series for CEV model. 71

3.3.9 Converged double-knock-out put for CEV model with various $K$. 72

3.3.10 Converged double-knock-out put values with various $T$. 72

3.3.11 Double-knock-out put for CEV model with $L \leq H \leq K$. 73

3.3.12 Convergence of double knock-out put for CEV model with various $T$. 74

4.1.1 Double-knock-out call Delta values. 77

4.1.2 Converged up-and-out call Delta curve. 78

4.2.1 Double-knock-out call Theta values. 79

4.2.2 Converged up-and-out call Theta values. 80

# Introduction

Derivative contracts or options can be broadly classified into two main categories: (*i*) non-path-dependent (European vanilla options) or (*ii*) path-dependent (Exotic options). Most standard equity options, such as European calls and puts, are of type (*i*).

Derivatives of type (*ii*) encompass a wide variety of modern-day contracts that are formulated within various markets that include equity, fixed-income and credit markets. Within the equity derivative arena, the basic difference between options of type (*i*) and type (*ii*) is either the inclusion of an early exercise feature (ie. American) or a more strongly path-dependent option feature whereby the payoff is a function of the history of the stock process, as in lookback or barrier options. Some contracts combine both features, and this gives rise to so called American style, lookback style and barrier options. This thesis focusses on the pricing of European style barrier options on a stock with fixed expiration date. These options come in various flavors: single or double-barrier, knock-in or knock-out, constant or time dependent barrier levels, etc. The characteristics of such options are well known [see Albanese and Campolieti 2005]. Chapter 3 of this thesis contains a description of knock-out options with constant barrier levels. As the name suggests, a single barrier knock-out option expires worthless if the stock price hits a predetermined single upper or lower level, in the case of a double-barrier knock-out, if the stock price reaches either level before

expiration. A nonzero payoff results only under scenarios in which the stock price does not attain the barrier(s) throughout the lifetime of the option. The payoffs are typically call-like or put-like. Knock-in barrier options have a complementary payoff structure and are hence valued by knock-in/knock-out symmetry, i.e. the valuation problem is reduced to that of the knock-out barrier option.

In the study of stochastic diffusion processes with application to finance, geometric Brownian motion is among the simplest models for continuous time asset pricing. In the GBM model, the asset price process is assumed to have a linear drift and a constant local volatility (i.e. $dS_t = \mu S_t dt + \sigma S_t dW_t$). For many years the GBM model was one of the few known continuous diffusion models to admit exact pricing formulas for various options, such as lookback and barrier European options. However, in the real world the volatility is not constant across maturities. The *constant elasticity of variance* (CEV) diffusion model is the first model to incorporate a nonlinear local volatility. The Laplace transform and spectral expansion approaches [see Davydov and Linesky 2001, Linetsky 2004] are useful for deriving analytical pricing formulas for CEV and other nonlinear volatility diffusion models.

In recent years, there was a new development in the construction of various new families of solvable multi-parameter nonlinear local volatility diffusion models that have a wide range of applicability in finance (see Albanese and Campolieti 2005, Campolieti and Makarov 2006, Campolieti 2008). The main idea in this new development is the use of a so-called *diffusion canonical transformation methodology.* The method allows us to map

more complex families of diffusions (we name them F-diffusions) into simpler families of diffusions (we name the latter $X$-diffusions). In particular, the approach allows us to develop analytically exact transition probability densities for new families of diffusions of interest (i.e. for F-diffusions) based on analytically exact transition probability densities that are readily obtained for underlying $X$-diffusions using Green's functions and spectral expansions. The diffusion canonical transformation methodology is applicable to general choices of underlying $X$-diffusions. However, in this thesis we focus exclusively on so-called *Bessel families* of nonlinear local volatility models with linear drift. These processes are generated by choosing the squared Bessel process as the $X$-diffusion.

In particular, we consider a new family of models referred to as the *drifted Bessel-K* diffusion processes. We use this subfamily of diffusions as a basis for describing asset (stock) price processes. The drifted Bessel-$K$ diffusions consist of four freely adjustable parameters, and for all choices of these parameters the processes describe discounted asset prices as martingales within an assumed risk-neutral measure. The local volatility of this Bessel family is highly nonlinear and consists of various desirable features that are observed in the equity options markets. Such features include the leverage effect at lower values of the asset price and pronounced smiles and skews in the implied volatility surface. Moreover, the Bessel-$K$ models are supersets of the CEV model, i.e. the driftless CEV model is recovered as a special limiting case of the Bessel-$K$ model. In this thesis, we tackle the problem of deriving new analytically exact pricing formulas for barrier options written on an underlying asset (stock) price process that is modeled according to a Bessel-$K$ diffusion.

The thesis is organized as follows. Chapter 1 provides the background for deriving closed-form spectral expansions for the transition probability density of an underlying solvable $X$-diffusion. The chapter presents the basic Green's function method and Sturm-Liouville formalism. Included in Chapter 1 are analytically exact spectral expansions for transition probability densities of a squared Bessel diffusion process with killing at one or two barriers. Chapter 2 presents the essential features of the diffusion canonical transformation methodology. This methodology leads to the construction of a new drifted Bessel family of diffusions, i.e. the drifted Bessel-$K$ and Bessel-$I$ diffusions with four parameters contained in the nonlinear local volatility function. Moreover, Chapter 2 also contains a brief introduction of the first hitting time for diffusions. The latter are used partly to derive barrier pricing formulas in Chapter 3. Chapter 3 presents derivations of new analytically exact pricing formulas for various standard European barrier options. This includes double knock-out, down-and-out and up-and-out call (and put) options. Moreover, we compare these results with those of the well-known GBM model. In addition, we recover the zero-drift CEV volatility model from the Bessel-$K$ subfamily and present various pricing results for the CEV. Finally, in Chapter 4 we investigate the sensitivity of barrier option prices under the drifted Bessel-$K$ model. That is, we compute the so-called "Greeks" for the European barrier call options which include the Delta and Theta of the option.

CHAPTER 1

# Spectral Expansion For Underlying Processes

## 1.1. Transition Density and Fundamental Solutions

Consider a one-dimensional time-homogeneous diffusion process $(X_t)_{t\geq 0}$ on the state space $\mathcal{D} = (l, r)$ with two endpoints, $l \geq -\infty$ and $l < r \leq \infty$, and obeying the stochastic differential equation

$$dX_t = \alpha(X_t)dt + \nu(X_t)dW_t,\ X_0 = x_0 \in \mathcal{D} \tag{1.1.1}$$

$(W_t)_{t\geq 0}$ is a one-dimensional standard Brownian motion and the $X$-process starts at $x_0$ at time $t = 0$. The drift function $\alpha(x)$ is assumed to be continuous and differentiable on $\mathcal{D}$. The volatility function $\nu(x)$ is assumed to be twice continuously differentiable on $\mathcal{D}$.

Let $u(x, x_0, t)$ be a transition density of the $X$ process. The transition probability density $u(x, x_0, t)$ hence satisfies the time-homogeneous forward Kolmogorov equation

$$\frac{\partial u}{\partial t} = \frac{1}{2}\frac{\partial^2}{\partial x^2}\left(\nu^2(x)u\right) - \frac{\partial}{\partial x}\left(\alpha(x)u\right) \equiv \mathcal{H}_x u \tag{1.1.2}$$

and the backward Kolmogorov equation

$$\frac{\partial u}{\partial t} = \frac{1}{2}\nu^2(x_0)\frac{\partial^2 u}{\partial x_0^2} + \alpha(x_0)\frac{\partial u}{\partial x_0} \equiv \mathcal{G}_{x_0} u \tag{1.1.3}$$

with initial condition $u(x, x_0, 0^+) = \delta(x - x_0)$, where $\delta(x - x_0)$ is the Dirac delta function. The operator $\mathcal{H}_x$ is the Fokker-Planck differential operator

which acts on variable $x$ and $\mathcal{G}_{x_0}$ is the generator (Lagrange adjoint operator) acting on $x_0$. The transition density $u(x, x_0, t)$ of the $X$-diffusion process is obtained by solving either forward or backward Kolmogorov partial differential equation.

For convenience, we introduce the speed density $\mathfrak{m}(x)$ and scale density $\mathfrak{s}(x)$ functions:

$$\mathfrak{s}(x) = \exp\left(-\int^x \frac{2\alpha(z)}{\nu^2(z)}dz\right), \qquad \mathfrak{m}(x) = \frac{2}{\mathfrak{s}(x)\nu^2(x)} \tag{1.1.4}$$

Then the operator in equation (1.1.2) and (1.1.3) take the compact forms in terms of speed and scale densities:

$$\mathcal{G}_x f = \frac{1}{\mathfrak{m}(x)}\left(\frac{f'}{\mathfrak{s}(x)}\right)', \quad \mathcal{H}_x f = \left(\frac{1}{\mathfrak{s}(x)}\left(\frac{f}{\mathfrak{m}(x)}\right)'\right)' \tag{1.1.5}$$

The ordinary differential equation

$$\mathcal{G}_x\varphi(x) = s\varphi(x), \; s \in \mathbb{C}, \; x \in \mathcal{D} \tag{1.1.6}$$

allows two linearly independent (fundamental) solutions $\varphi_s^+(x)$ and $\varphi_s^-(x)$, for $\mathrm{Re}(s) > 0$ and subject to appropriate boundary conditions. For positive value $\rho$ (i.e. $\rho = \mathrm{Re}(s) > 0$), the fundamental solutions $\varphi_\rho^+(x)$ and $\varphi_\rho^-(x)$ are strictly increasing and decreasing, respectively (see Borodin and Salminen 2000, Karlin and Talylor 1981). The boundary points $\{l, r\}$, the diffusions $(X_t)_{t\geq 0}$, can be either regular, natural, entrance or exit (see Linetsky 2004). For regular boundaries, the diffusions $(X_t)_{t\geq 0}$, are either killing (or absorbing) upon hitting the boundaries points or instantaneous reflecting. For instantaneous reflection boundaries, the boundaries points are included in the state space. On the other hand, for the other types of boundaries, the

endpoints are excluded from the state space. In this thesis we only consider the regular killing boundary conditions. The fundamental solutions $\varphi_s^{\pm}(x)$ satisfy the homogeneous endpoints regular killing boundary conditions:

$$\lim_{x\to r^-} \frac{\varphi_\rho^+(x)}{\varphi_\rho^-(x)} = \infty \text{ and } \lim_{x\to l^+} \frac{\varphi_\rho^+(x)}{\varphi_\rho^-(x)} = 0 \tag{1.1.7}$$

The Wronskian of fundamental solutions can be computed as:

$$W[\varphi_s^-, \varphi_s^+](x) := \varphi_s^-(x)\frac{d}{dx}\left(\varphi_s^+(x)\right) - \varphi_s^+(x)\frac{d}{dx}\left(\varphi_s^-(x)\right) = w_s \mathfrak{s}(x) \tag{1.1.8}$$

where $w_s$ is a constant with respect to $x$.

First note that the operator $\mathcal{L} := -\mathcal{G}$, where $\mathcal{L}$ is a Sturm-Liouville operator, and hence equation (1.1.6) can be written as

$$\mathcal{L}_x \varphi(x) = \lambda \varphi(x) \tag{1.1.9}$$

where we set $\lambda = -s$. The linear independent solution set becomes $\varphi_{-\lambda}^{\pm}(x)$ on the space $L^2(m, (l, r))$.

Consider the Green's function $G(x, x_0, s)$ for finding the transition probability density $u(x, x_0, t)$ for the $X$-diffusion with homogenous boundary conditions. The Green's function $G(x, x_0, s)$ is defined by the Laplace transform

$$G(x, x_0, s) = L[u(x, x_0, t)](s) = \int_0^\infty e^{-st} u(x, x_0, t) dt, \ s \in \mathbb{C} \tag{1.1.10}$$

The transition probability density $u(x, x_0, t)$ satisfies the same homogenous boundary conditions as $G(x, x_0, s)$, and is obtained by the following inverse Laplace transformation:

$$u(x, x_0, t) = L^{-1}[G(x, x_0, s)](t) \tag{1.1.11}$$

From Sturm-Liouville theory, the spectral expansion of a transition density fall into three main categories (see Campolieti 2008, Davydov and Linetsky), *spectral category I*, *spectral category II*, *spectral category III*. Throughout this thesis we only need to consider *spectral category I*, i.e. the spectrum is simple, nonnegative and purely discrete. This corresponds to the case where $G(x, x_0, s)$ has simple poles at $s = -\lambda_n, n = 1, 2, \cdots, \infty$. These form countably infinite set $\{\lambda_n\}_{n=1}^{\infty}$ with an increasing unique sequence $0 < \lambda_1 < \lambda_2 < \lambda_3 < \cdots$, with $\lambda_n \to \infty$ as $n \to \infty$. Therefore, the Green's function $G(x, x_0, s)$ takes on the form of spectral expansion

$$G(x, x_0, \lambda = -s) = \mathfrak{m}(x) \sum_{n=1}^{\infty} \frac{\phi_n(x)\phi_n(x_0)}{s + \lambda_n} \tag{1.1.12}$$

where $\phi_n(x)$ are the eigenfunctions corresponding to $\lambda_n$. These satisfy

$$\mathcal{L}_x \phi_n(x) = \lambda_n \phi_n(x), \ n = 1, 2, \cdots \tag{1.1.13}$$

and form a complete orthonormal basis with inner product:

$$\langle \phi_n(x), \phi_m(x) \rangle_{[a,b]} := \int_a^b \mathfrak{m}(x)\phi_m(x)\phi_n(x)dx = \delta_{mn} \tag{1.1.14}$$

with speed density $\mathfrak{m}(x)$ defined in equation (1.1.4).

The transition probability density $u(x, x_0, t)$, is obtained by taking the inverse Laplace transform of equation (1.1.10) with Green's function $G(x, x_0, s)$ is given in equation (1.1.12). This leads to:

$$\begin{aligned} u(x, x_0, t) &= \mathfrak{m}(x) \sum_{n=1}^{\infty} \phi_n(x)\phi_n(x_0) L^{-1}\left[\frac{1}{s + \lambda_n}\right](t) \\ &= \mathfrak{m}(x) \sum_{n=1}^{\infty} e^{-\lambda_n t}\phi_n(x)\phi_n(x_0) \end{aligned} \tag{1.1.15}$$

In this thesis we are interested in diffusion processes with killing at two arbitrary finite endpoints, $x = x_L$ and $x = x_H$ (i.e. $X_t \in [x_L, x_H]$ where $x_L < x_H$). The process with killing at a single arbitrary finite endpoint, either upper $x = x_H$ or lower $x = x_L$, can be obtained by taking appropriate limits, i.e. $\lim_{x_L \to l+}$ for the process killed at $x = x_H$ and $\lim_{x_H \to r-}$ for the process killed at $x = x_L$. The transition probability density with two barrier endpoints, $x_L$ and $x_H$, is denoted by $u(x, x_0, x_L, x_H, t)$. Hence, the zero homogenous boundary conditions at two finite endpoints, $x_L$ and $x_H$, imposed on a transition density $u(x, x_0, x_L, x_H, t)$ read as

$$u(x_L, x_0, x_L, x_H, t) = u(x_H, x_0, x_L, x_H, t) = 0 \tag{1.1.16}$$

By imposing homogenous boundary conditions on the transition probability density $u(x, x_0, x_L, x_H, t)$, the eigenfunctions $\phi_n(x)$ (corresponding to eigenvalues $\lambda_n$) satisfy equation (1.1.13) with boundary condition $\phi(x_L) = \phi(x_H) = 0$ and inner product in equation (1.1.14). This gives (see Campolieti 2008)

$$\phi_n(x) = \pm \frac{f(x, x_H; -\lambda_n)}{\sqrt{A_n C_n}} \tag{1.1.17}$$

where $A_n$ and $C_n$ are defined as follows:

$$\begin{aligned} A_n &= -\frac{\varphi^+_{-\lambda_n}(x_H)}{\varphi^+_{-\lambda_n}(x_L)} \\ C_n &= \frac{1}{\mathfrak{s}(x)} \frac{d}{dx} \left( w_s \mathfrak{s}(x) f(x_L, x_H; s) \right) |_{s=-\lambda_n} \end{aligned} \tag{1.1.18}$$

and a cylinder function $f(x, x_H; -\lambda_n)$ given as

$$f(x, y; -\lambda_n) = \varphi^-_{-\lambda_n}(x)\varphi^+_{-\lambda_n}(y) - \varphi^-_{-\lambda_n}(y)\varphi^+_{-\lambda_n}(x) \tag{1.1.19}$$

The eigenvalues $\lambda_n$ are the simple zeros solving $f(x_L, x_H; -\lambda_n) = 0$.

## 1.2. Squared Bessel Process

Suppose we have a regular one-dimensional squared Bessel diffusion process $(X_t)_{t\geq 0} \in \mathcal{D} = (l, r) = (0, \infty)$ which obeys the stochastic differential equation

$$dX_t = \alpha_0 dt + 2\sqrt{X_t} dW_t \tag{1.2.1}$$

where $\alpha_0$ is a constant. Assume that the process $X_0$ starts at $x_0 \in \mathcal{D}$ and we define $\mu \equiv \alpha_0/2 - 1 > 0$. From equation (1.1.4) given in the previous section, we obtain the speed and scale densities:

$$\mathfrak{m}(x) = \frac{x^\mu}{2}, \quad \mathfrak{s}(x) = x^{-\mu-1} \tag{1.2.2}$$

The fundamental solutions, $\varphi_s^+(x)$ and $\varphi_s^-(x)$ for $s \in \mathbb{C}$, to the homogenous ordinary differential equation (1.1.9) are given as

$$\varphi_s^+(x) = x^{-\mu/2} I_\mu(\sqrt{2sx}), \quad \varphi_s^-(x) = x^{-\mu/2} K_\mu(\sqrt{2sx}) \tag{1.2.3}$$

The functions $I_\mu(z)$ and $K_\mu(z)$ are the first and second kind of modified Bessel functions with order $\mu$, respectively (see Abramowitz and Stegun), and satisfy a Wronskian relation as in (1.1.8) with $w_s = 1/2$. Using the small and large argument asymptotics of the modified Bessel functions $I_\mu(z)$ and $K_\mu(z)$, we readily show that $\varphi_s^\pm(x)$ satisfy the boundary conditions in (1.1.7). Note that, at the boundary point $l = 0$, the squared Bessel process has entrance for $\mu \geq 0$, exit for $\mu \leq -1$ and regular killing for $\mu \in (-1, 0)$. Similarly, at the boundary $r = \infty$, the process is attracting for $\mu > 0$. In this thesis we only consider the case where $\mu > 0$.

From equation (1.1.15) and the speed density $\mathfrak{m}(x)$ defined in equation (1.1.4), we obtain an exact double-barrier transition density, $u(x, x_0, x_L, x_H, t)$,

with lower level $x_L > 0$ and upper level $x_H < \infty$ of a squared Bessel diffusion process. That is, the transition probability density for the squared Bessel process with killing at both endpoints $x_L < x_H$ is:

$$\begin{aligned} u(x, x_0, x_L, x_H, t) &= \mathfrak{m}(x) \sum_{n=1}^{\infty} e^{-\lambda_n t} \phi_n(x) \phi_n(x_0) \\ &= \left(\frac{x^\mu}{2}\right) \sum_{n=1}^{\infty} e^{-\lambda_n t} \phi_n(x) \phi_n(x_0) \end{aligned} \tag{1.2.4}$$

The eigenfunctions $\phi_n(x)$ are obtained via equations (1.1.17), (1.1.18), (1.1.19) and (1.2.3). Upon using the identities $I_\mu(ix) = i^\mu J_\mu(x)$ and $K_\mu(ix) = i^{-\mu}(\pi/2)[Y_\mu(x) - iJ_\mu(x)]$, for $x \in \mathbb{R}$ gives

$$\phi_n(x) = \mathcal{N}_n x^{-\mu/2} f_\mu(x, x_L, \lambda_n) \tag{1.2.5}$$

Here we define a normalization constant $\mathcal{N}_n$, and a Bessel cylinder function $f_\mu(x, y, \lambda_n)$, as follows

$$\begin{aligned} f_\mu(x, y, \lambda_n) &= \left[J_\mu(\sqrt{2\lambda_n y}) Y_\mu(\sqrt{2\lambda_n x}) - Y_\mu(\sqrt{2\lambda_n y}) J_\mu(\sqrt{2\lambda_n x})\right], \\ \mathcal{N}_n &= \pi\sqrt{\lambda_n} \left[\frac{Y_\mu^2(\sqrt{2\lambda_n x_L})}{Y_\mu^2(\sqrt{2\lambda_n x_H})} - 1\right]^{-1/2} \end{aligned} \tag{1.2.6}$$

The functions $J_\mu(z)$ and $Y_\mu(z)$ are the ordinary Bessel functions of the first and second kind with order $\mu > 0$. The corresponding eigenvalues $\lambda_n$ are the positive simple zeros of the cylinder functions

$$f_\mu(x_L, x_H, \lambda_n) = 0, \; n = 1, 2, \cdots, \infty \tag{1.2.7}$$

Using the asymptotic forms $J_\mu(z) \sim \sqrt{2/\pi z} \cos(z - \mu\pi/2 - \pi/4)$ and $Y_\mu(x) \sim \sqrt{2/\pi z} \sin(z - \mu\pi/2 - \pi/4)$ for a cylinder function $f_\mu(x_L, x_H, \lambda_n)$

as $\lambda_n \to \infty$, gives

$$f_\mu(x_L, x_H, z) \sim \frac{\sqrt{2}(x_L x_H)^{-1/4}}{\pi\sqrt{z}} \sin\left(\sqrt{z}(\sqrt{2x_L} - \sqrt{2x_H})\right),\ z \to \infty \quad (1.2.8)$$

Hence, the eigenvalues $\lambda_n$ can be approximated as

$$\lambda_n \sim z_n = \frac{n^2\pi^2}{2(\sqrt{x_H} - \sqrt{x_L})^2},\ n = 1, 2, \cdots, \infty \quad (1.2.9)$$

Note that we use $z_n$ as an initial guess in obtaining numerically exact values of $\lambda_n$. The exact values of $\lambda_n$ were obtained using the Matlab built-in fzero function.

Similarly, the squared Bessel diffusion with killing at a single upper barrier $x_H$ (i.e. $(X_t)_{t\geq 0} \in (0, x_H]$) falls in the *spectral category I* (i.e. simple, nonnegative and purely discrete spectrum). The closed-form upper barrier transition probability density, denoted by $u(x, x_0, x_H, t)$, takes on the form of equation (1.1.15) with normalized eigenfunctions (see Campolieti 2008)

$$\phi_n(x) = \frac{x^{-\mu/2} J_\mu(\sqrt{2\lambda_n x})}{\sqrt{x_H/2} J_{\mu+1}(\sqrt{2\lambda_n x_H})} \quad (1.2.10)$$

An accurate initial guess for the eigenvalues $\lambda_n$ follows from the asymptotic form for $J_\mu(z)$ as $z \to \infty$, i.e. the simple zeros solving $J_\mu(\sqrt{2\lambda_n x_H}) = 0$ are approximated as

$$\lambda_n \sim \frac{\pi}{4x_H}\left[(2n + \mu) - 1/2\right]^2 \quad (1.2.11)$$

Another approach for computing single barrier transition densities follows by taking limits as $x_L$ approaches zero (for single upper barrier $x_H$) or as $x_H$ approaches infinity (for single lower barrier $x_L$) within the double-barrier transition density. In chapter 4, we will develop single barrier pricing formulas for the drifted Bessel-$K$ family by using such a limiting approach.

This limiting approach is particularly useful for the case of the single lower barrier problem which has a purely continuous positive spectrum.

CHAPTER 2

# Spectral Expansions for Transformed F-Diffusions

## 2.1. Canonical Transformation Methodology

In this section, we derive families of new diffusions (i.e. so-called F-diffusions) which are obtained via the *diffusion canonical transformation* methodology (see Albanese and Campolieti 2005, Campolieti and Makarov 2006, Campolieti 2008). One of the basic ideas is to consider the so-called $X$-diffusions where the transition densities can be solved analytically by a Green's function technique. Then, the pricing kernels (transition probability densities) of F-diffusions are related to those of the $X$-diffusions.

Consider a one-dimensional time-homogenous regular diffusion process $(X^{(\rho)})_{t\geq 0} \in (l, r)$ with a parameter $\rho > 0$, defined by the generator

$$\mathcal{G}^{(\rho)} f(x) := \frac{1}{2}\nu^2(x)\frac{d^2 f(x)}{dx^2} + \left(\alpha(x) + \nu^2(x)\frac{\hat{u}'(x,\rho)}{\hat{u}(x,\rho)}\right)\frac{df(x)}{dx} \qquad (2.1.1)$$

where $\hat{u}'(x,\rho) = \frac{d\hat{u}(x,\rho)}{dx}$ and $\hat{u}(x,\rho)$ is defined in (2.1.3). $\alpha(x)$ and $\nu(x)$ are the drift and diffusion coefficients of the $X$-diffusion given in equation (1.1.1). The $X^{(\rho)}$-diffusions can be viewed as satisfying the stochastic differential equation

$$dX_t^{(\rho)} = \alpha^{(\rho)}(X_t^{(\rho)})dt + \nu^{(\rho)}(X_t^{(\rho)})dW_t \qquad (2.1.2)$$

where $\alpha^{(\rho)}(x) := \alpha(x) + \nu^2(x)\frac{\hat{u}'(x,\rho)}{\hat{u}(x,\rho)}$ and $\nu^{(\rho)}(x) := \nu(x)$. The transformations from $X_t$ to $X_t^{(\rho)}$ processes are described in much more detail in Campolieti and Makarov 2006, 2008, Campolieti 2008.

For real values $s = \rho > 0$, the homogenous ordinary differential equation (1.1.6) admits a set of linearly independent solutions, $\varphi_\rho^+(x)$ and $\varphi_\rho^-(x)$. We define a generating function $\hat{u}(x,\rho)$ as

$$\hat{u}(x,\rho) = q_1\varphi_\rho^+(x) + q_2\varphi_\rho^-(x) \tag{2.1.3}$$

where $q_1, q_2$ are parameters and at least one of them is assumed to be strictly positive.

The transition probability density function of an $X^{(\rho)}$-diffusion, denoted by $u^{(\rho)}(x, x_0, t)$, is related to that of the $X$-diffusion:

$$u^{(\rho)}(x, x_0, t) = e^{-\rho t}\frac{\hat{u}(x,\rho)}{\hat{u}(x_0,\rho)}u(x, x_0, t) \tag{2.1.4}$$

The speed and scale densities of the $X^{(\rho)}$-diffusion are defined as

$$\mathfrak{m}^{(\rho)}(x) := \hat{u}^2(x,\rho)\mathfrak{m}(x), \quad \mathfrak{s}^{(\rho)}(x) := \frac{\mathfrak{s}(x)}{\hat{u}^2(x,\rho)} \tag{2.1.5}$$

Now consider a (new) one-dimensional regular F-diffusion $(\mathrm{F}_t)_{t\geq 0}$ defined via a strictly monotonic mapping of an $X^{(\rho)}$-diffusion, i.e. $\mathrm{F}_t = \mathsf{F}(X_t^{(\rho)})$. The diffusion process has regular state space $(\mathrm{F}_t)_{t\geq 0} \in \widetilde{\mathcal{D}} = (F^{(l)}, F^{(r)})$, where $F^{(l)} = \min\{\mathsf{F}(l+), \mathsf{F}(r-)\}$ and $F^{(r)} = \max\{\mathsf{F}(l+), \mathsf{F}(r-)\}$ are left and right endpoints of $\widetilde{\mathcal{D}}$, respectively. Throughout we assume that the mapping $F = \mathsf{F}(x)$ is continuous and twice differentiable for all $x$ in $\mathcal{D} = (l, r)$ and that the process $(\mathrm{F}_t)_{t\geq 0}$ obeys the stochastic differential equation

$$d\mathrm{F}_t = \theta\mathrm{F}_t dt + \sigma(\mathrm{F}_t)dW_t, \ \mathrm{F}_0 = F_0 \tag{2.1.6}$$

where $(W_t)_{t\geq 0}$ is a standard Brownian motion and $\theta$ is a constant.

As discussed in Albanese et al. 2001, Albanese and Campolieti 2005, Campolieti and Makarov 2006, Campolieti 2008, the *diffusion canonical transformation* methodology gives

$$\frac{d\mathsf{X}}{dF} = \pm\frac{\nu(x)}{\sigma(F)} \tag{2.1.7}$$

and a volatility function

$$\sigma(F) = \nu(x)\frac{|W[\hat{v}(x,\rho+\theta),\hat{u}(x,\rho)]|}{[\hat{u}(x,\rho)]^2} \tag{2.1.8}$$

where $x = \mathsf{X}(F) := \mathsf{F}^{-1}(F)$ is an inverse mapping of $F = \mathsf{F}(x)$, as follows by equation (2.1.7) and $\hat{u}(x,\rho)$ is given in (2.1.3). The signs $\pm$ in equation (2.1.7) permit two possible maps. A negative sign $(-)$ gives a monotonically decreasing map and a positive sign $(+)$ provides a monotonically increasing map. For $\rho+\theta > 0$, we define $\hat{v}(x,\rho+\theta)$ as

$$\hat{v}(x,\rho+\theta) = [c_1\varphi^+_{\rho+\theta}(x) + c_2\varphi^-_{\rho+\theta}(x)] \tag{2.1.9}$$

where $c_1$ and $c_2$ are real constants, and one of them is assumed to be strictly nonzero.

Now, using the relationship between equations (2.1.7) and (2.1.8), we achieve the mapping $F = \mathsf{F}(x)$

$$\mathsf{F}(x) = \frac{c_1\varphi^+_{\rho+\theta}(x) + c_2\varphi^-_{\rho+\theta}(x)}{q_1\varphi^+_{\rho}(x) + q_2\varphi^-_{\rho}(x)} \tag{2.1.10}$$

where $c_i$ and $q_i$, for $i = 1,2$, are real parameters. By choosing appropriate values of parameters $q_i$ and $c_i$ in equation (2.1.10), the mapping yields different families of F-diffusions. That is, setting $q_1 = c_2 = 0, q_2 = 1, c_1 =$

$a > 0$, $F = \mathsf{F}(x)$ gives a monotonically increasing map, and similarly, setting $q_1 = 1, q_2 = c_1 = 0, c_2 = a > 0$ $F = \mathsf{F}(x)$ leads to a monotonically decreasing map. Two (dual) families of diffusions arise as follows:

(1) Monotonically increasing maps and volatility function:
- $\sigma(F) = a\dfrac{\nu(x)W[\varphi_\rho^-(x), \varphi_{\rho+\theta}^+(x)]}{[\varphi_\rho^-(x)]^2}, \quad a > 0$
- $\mathsf{F}(x) = a\dfrac{\varphi_{\rho+\theta}^+(x)}{\varphi_\rho^-(x)}$
- $\hat{u}(x,\rho) = \varphi_\rho^-(x)$

(2) Monotonically decreasing map and volatility function:
- $\sigma(F) = a\dfrac{\nu(x)W[\varphi_{\rho+\theta}^-(x), \varphi_\rho^+(x)]}{[\varphi_\rho^+(x)]^2}, \quad a > 0$
- $\mathsf{F}(x) = a\dfrac{\varphi_{\rho+\theta}^-(x)}{\varphi_\rho^+(x)}$
- $\hat{u}(x,\rho) = \varphi_\rho^+(x)$

The transition probability density of an F-diffusion, denoted by $U(F, F_0, t)$, is related to that of an $X^{(\rho)}$-diffusion (or $X$-diffusion) as

$$\begin{aligned} U(F, F_0, t) &= |\mathsf{X}'(F)| u^{(\rho)}(\mathsf{X}(F), \mathsf{X}(F_0), t) \\ &= \frac{\nu(\mathsf{X}(F))}{\sigma(F)} \frac{\hat{u}(\mathsf{X}(F), \rho)}{\hat{u}(\mathsf{X}(F_0), \rho)} e^{-\rho t} u(\mathsf{X}(F), \mathsf{X}(F_0), t) \end{aligned} \tag{2.1.11}$$

The transition densities of the F-diffusions with killing, at either single or double barrier(s), are obtained by directly substituting either a single or a double barrier transition density $u(x, x_0, t)$ for the underlying $X$-diffusion.

## 2.2. First Hitting Time

The main objective of this thesis is to develop barrier pricing formulas for the stock price process modeled by the new F-diffusions. For this reason, it is important to introduce the first hitting time concept, i.e. the first time that the process $\mathrm{F}_t$ crosses a particular barrier either from below or above.

In what follows we shall only consider F-diffusions on the regular state space $\widetilde{\mathcal{D}} = (F^{(l)}, F^{(r)}) \equiv (0, \infty)$.

Consider the F-diffusions defined in (2.1.6) with killing at any real value $b \in (0, \infty)$. We denote the first hitting time of the process $\mathrm{F}_t$ at level $b$, *either from above or below*, by $\tau_b^*$, and it is defined by

$$\tau_b^* = \inf \{t \geq 0 | \mathrm{F}_t = b, F_0 \in (0, \infty)\} \tag{2.2.1}$$

Also, we consider the process $\mathrm{F}_t^{(L,H)}$: the F-diffusions defined in (2.1.6) with killing at two barriers, upper barrier $H < \infty$ and lower barrier $L > 0$. We assume that the process starts at $F_0 \in [L, H]$. We denote the first hitting time for reaching the lower barrier $L$ and the first hitting time for reaching the upper barrier $H$ by $\tau_L$ and $\tau_H$, respectively. We hence define $\tau_L$ and $\tau_H$ as follows:

$$\begin{aligned} \tau_L &= \inf\{t \geq 0 | \mathrm{F}_t = L, F_0 \in [L, H]\} \\ \tau_H &= \inf\{t \geq 0 | \mathrm{F}_t = H, F_0 \in [L, H]\} \end{aligned} \tag{2.2.2}$$

If an F-diffusion hits either $L$ or $H$, then it is absorbed (or killed) and sent to the so-called cemetary state $o$. If $\mathrm{F}_t \in (L, H)$, (i.e. $\tau_L, \tau_H < t$), we have $\mathrm{F}_t^{(L,H)} = \mathrm{F}_t$. We can rewrite the process $\mathrm{F}_t^{(L,H)}$, killed at both barrier levels $L$ and $H$ in the compact form:

$$\mathrm{F}_t^{(L,H)} = \begin{cases} o, & \text{if } \tau_L \text{ or } \tau_H \leq t; \\ \mathrm{F}_t, & \text{if } \tau_L, \tau_H > t. \end{cases} \tag{2.2.3}$$

The process with a single absorbing barrier can be obtained by a limiting approach. That is, taking the limit $L \to 0^+$ of $\mathrm{F}_t^{(L,H)}$ gives a F-diffusion with a single killing upper barrier at $H$, and limit $H \to \infty$ of $\mathrm{F}_t^{(L,H)}$ leads

to a F-diffusion with imposed killing at lower level $L$. The barrier-free case arises when $L \to 0^+$ and $H \to \infty$.

For the purpose of pricing barrier options, to follow in chapter three, we define $\tau_L^-(H)$, the *first hitting time down* of the process $\mathrm{F}_t$ for barrier level $L$ conditional on the process reaching $L$ before level $H$, given that the process starts at $\mathrm{F}_0 = F_0 \in (L, H)$ (see figure 2.2.1). Similarly, we define $\tau_H^+(L)$ as the *first hitting time up* at $H$ before hitting level $L$, given that the process starts at $\mathrm{F}_0 = F_0 \in (L, H)$. Hence, $\tau_L^-(H)$ and $\tau_H^+(L)$ are defined as:

$$\begin{aligned} \tau_L^-(H) &= \inf\{t \geq 0 | \mathrm{F}_t = L, M_t < H, F_0 \in (L, H)\} \\ \tau_H^+(L) &= \inf\{t \geq 0 | \mathrm{F}_t = H, m_t > L, F_0 \in (L, H)\} \end{aligned} \tag{2.2.4}$$

where $M_t$ and $m_t$ are defined to be the realized maximum and minimum of the process up to time $t$:

$$M_t = \sup_{0 \leq s \leq t} \mathrm{F}_s, \quad m_t = \inf_{0 \leq s \leq t} \mathrm{F}_s \tag{2.2.5}$$

Therefore, from equations (2.2.2) and (2.2.4), for $F_0 \in (L, H)$, we have the following probability relations

$$\mathbb{P}\{\tau_L < \tau_H, \tau_L \leq t\} = \mathbb{P}\{\tau_L^-(H) \leq t\} \tag{2.2.6}$$

and

$$\mathbb{P}\{\tau_H < \tau_L, \tau_H \leq t\} = \mathbb{P}\{\tau_H^+(L) \leq t\} \tag{2.2.7}$$

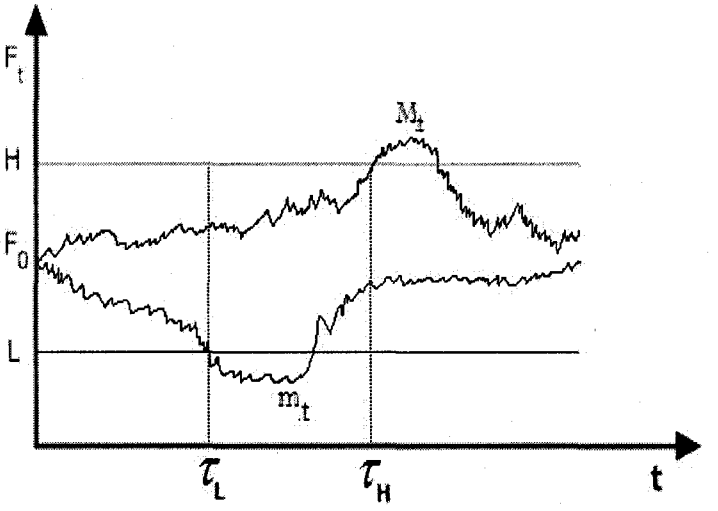


Figure 2.2.1: Typical paths depicting first hitting times.

## 2.3. Drifted Bessel Family of F-Diffusions

In this section we develop new families of F-diffusions satisfying equation (2.1.6), where the underlying diffusion $X_t$ is a squared Bessel process satisfying equation (1.2.1).

By directly substituting $\hat{v}(x, \rho+\theta)$ into equation (2.1.10), with $\hat{v}$ defined in equation (2.1.9), with $\hat{u}(x, \rho)$ given in equation (2.1.3) and the fundamental solutions $\varphi_\rho^{\pm}(x)$ given in equation (1.2.3), we obtain the general form for the Bessel mapping $F = \mathsf{F}(x)$, i.e.

$$\mathsf{F}(x) = \frac{c_1 I_\mu(\sqrt{2(\rho+\theta)x}) + c_2 K_\mu(\sqrt{2(\rho+\theta)x})}{q_1 I_\mu(\sqrt{2\rho x}) + q_2 K_\mu(\sqrt{2\rho x})} \tag{2.3.1}$$

The general form for the volatility function is

$$\sigma(F) = \nu(x)\frac{|W[c_1\varphi^+_{\rho+\theta}(x) + c_2\varphi^-_{\rho+\theta}(x), q_1\varphi^+_\rho(x) + q_2\varphi^-_\rho(x)]|}{[q_1\varphi^+_\rho(x) + q_2\varphi^-_\rho(x)]^2} \tag{2.3.2}$$

where $\varphi_\rho^{\pm}(x)$ are given in equation (1.2.3). The mapping $x = \mathsf{X}(F) := \mathsf{F}^{-1}(F)$ is the unique inverse given by inverting equation (2.3.1). Note that, in equations (2.3.1) and (2.3.2), the parameters $c_i$ and $q_i$ for $i = 1, 2$, are real nonnegative parameters such that either $q_1 > 0$ or $q_2 > 0$ and either $c_1 > 0$ or $c_2 > 0$.

Equation (2.3.2) gives a general form for the volatility function $\sigma(\mathrm{F})$ for all families of drifted Bessel diffusions. By setting the appropriate parameters $c_i$ and $q_i$, this reduces to different subfamilies. That is, setting $q_1 = 0, q_2 = 1, c_1 = a > 0$ and $c_2 = 0$ gives the so-called (four-parameter) Bessel $K$-subfamily. Similarly, setting $q_2 = 0, q_1 = 1, c_2 = a > 0$ and $c_1 = 0$ gives the so-called (four-parameter) Bessel $I$-subfamily.

The (dual) drifted Bessel $I$- and $K$-subfamilies are characterized as follows.

(1) Monotonically increasing map, Bessel $K$-subfamily:

$$\begin{cases} \dfrac{\sigma(\mathrm{F})}{\mathrm{F}} = \dfrac{\sqrt{2\rho}K_{\mu+1}(\sqrt{2\rho x})}{2K_\mu(\sqrt{2\rho x})} + \dfrac{\sqrt{2(\rho+\theta)}I_{\mu+1}(\sqrt{2(\rho+\theta)x})}{2I_\mu(\sqrt{2(\rho+\theta)x})} \\ \mathsf{F}(x) = a\dfrac{I_\mu(\sqrt{2(\rho+\theta)x})}{K_\mu(\sqrt{2\rho x})}, \quad a > 0 \\ \hat{u}(x,\rho) = x^{-\mu/2}K_\mu(\sqrt{2\rho x}) \end{cases} \tag{2.3.3}$$

(2) Monotonically decreasing map, Bessel $I$-subfamily:

$$\begin{cases} \dfrac{\sigma(\mathrm{F})}{\mathrm{F}} = \dfrac{\sqrt{2\rho}I_{\mu+1}(\sqrt{2\rho x})}{2I_\mu(\sqrt{2\rho x})} + \dfrac{\sqrt{2(\rho+\theta)}K_{\mu+1}(\sqrt{2(\rho+\theta)x})}{2K_\mu(\sqrt{2(\rho+\theta)x})} \\ \mathsf{F}(x) = a\dfrac{K_\mu(\sqrt{2(\rho+\theta)x})}{I_\mu(\sqrt{2\rho x})}, \quad a > 0 \\ \hat{u}(x,\rho) = x^{-\mu/2}I_\mu(\sqrt{2\rho x}) \end{cases} \tag{2.3.4}$$

The four adjustable parameters are $\rho, \theta, a, \mu$ such that $\rho, \rho + \theta, a, \mu$ are all strictly positive. In both cases, $x = \mathsf{X}(F)$ where $\mathsf{X} = \mathsf{F}^{-1}$ is given by the respective inverse map.

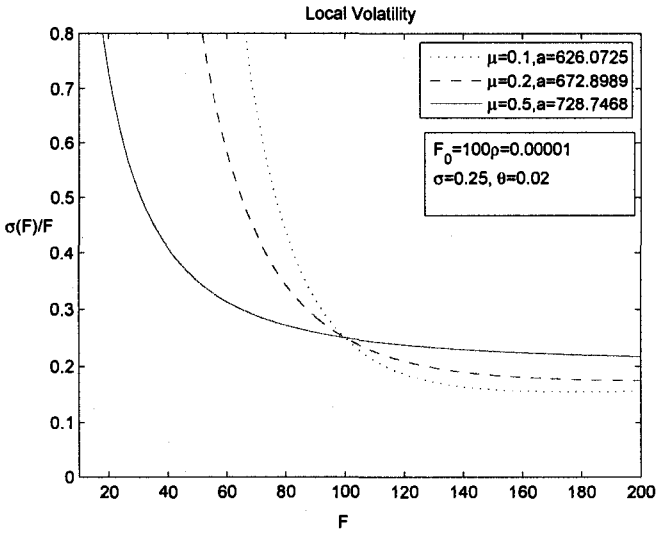


Figure 2.3.1: Typical local volatility curves for the Bessel $K$-subfamily.

Figure 2.3.1 displays typical local volatility curves, $\sigma(F)/F$ versus $F$, for the Bessel $K$-subfamily with fixed values $r(= \theta), \rho, \sigma := \sigma(F_0)/F_0 = 0.25$ for $F_0 = 100$, and various choices of parameters $(\mu, a)$. The parameters have been chosen such that the volatility function $\sigma(F)/F$ has a fixed value of 0.25 at $F = 100$. In contrast, Figure 2.3.2 shows local volatility functions for the Bessel $I$-subfamily with various choices of values $(\mu, a)$, where $\theta = 0.02(= r), \rho = 0.0125, \sigma := \sigma(F_0)/F_0 = 0.25$ for $F_0 = 2$. In both Figures, the model parameters have been chosen such that the local volatility function $\sigma(F)/F$ has a fixed value at some spot value $F = F_0$. It is apparent that the Bessel-$K$ model exhibits a pronounced leverage effect at smaller values

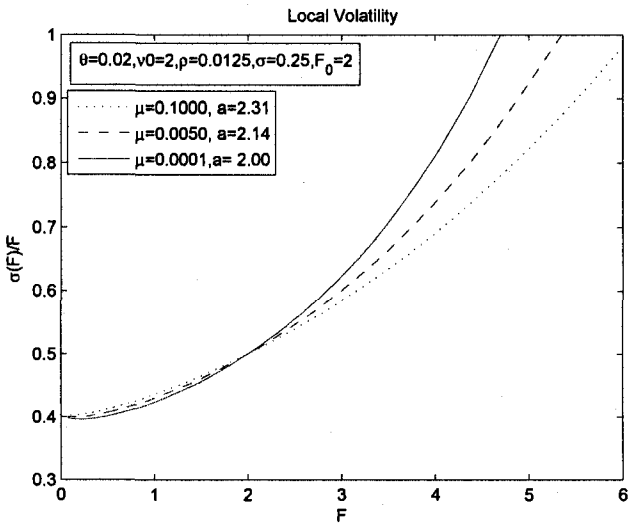


Figure 2.3.2: Typical local volatility curves for the Bessel $I$-subfamily.

of the asset price $F$. The relative steepness of the curves can be controlled by adjusting the model parameters.

## 2.4. Transition Density for Drifted Bessel-$K$ Family

In this section we present the transition probability density for the Bessel $K$-subfamily of F-diffusions with killing at two barriers. We denote this transition density by $U(F, F_0, L, H, t)$, where $L > 0$ and $H < \infty$ are lower and upper barriers, respectively.

The transition density is obtained by substituting the generating function, $\hat{u}(x, \rho)$ in (2.3.3), and the (double-barrier) transition density into equation (2.1.11). This gives an exact closed-form spectral expansion for the transition density:

$$U(F, F_0, L, H, t) = |\mathsf{X}'(F)| \frac{K_\mu(\sqrt{2\rho x})}{2K_\mu(\sqrt{2\rho x_0})} \sum_{n=1}^{\infty} e^{-(\rho+\lambda_n)t} \mathcal{N}_n^2 f_\mu(x_0, x_L, \lambda_n) f_\mu(x, x_L, \lambda_n) \tag{2.4.1}$$

where $|\mathsf{X}'(F)| = \nu(x)/\sigma(F) = 2\sqrt{x}/\sigma(F), x_L = \mathsf{X}(L), x_H = \mathsf{X}(H), x_0 = \mathsf{X}(F_0), x = \mathsf{X}(F)$ via equation (2.3.3). The normalization constant $\mathcal{N}_n$ and the cylinder function $f_\mu(x, y, \lambda_n)$ are given by equation (1.2.6). The end-points $x_L$ and $x_H$ are uniquely given by inverting

$$\begin{aligned} \mathsf{F}(x_L) = L &= a\frac{I_\mu(\sqrt{2(\rho+\theta)x_L})}{K_\mu(\sqrt{2\rho x_L})}, \\ \mathsf{F}(x_H) = H &= a\frac{I_\mu(\sqrt{2(\rho+\theta)x_H})}{K_\mu(\sqrt{2\rho x_H})} \end{aligned} \tag{2.4.2}$$

Since $\mathsf{F}(x)$ is a Bessel-$K$ map (i.e. monotonically increasing), then for all values $x$ and $x_0$ in $[x_L, x_H]$ we have $F, F_0 \in [L, H]$.

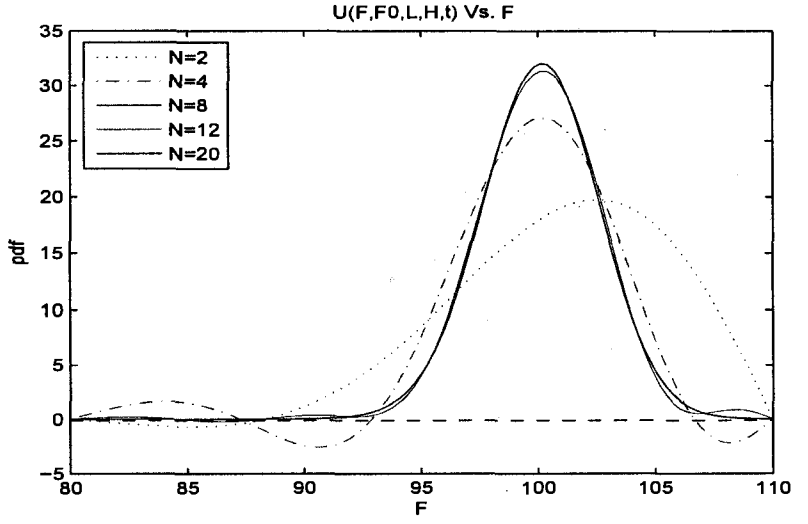


Figure 2.4.1: Rapid convergence of series in (2.4.1).

Figure 2.4.1 shows plots of the computed series in (2.4.1) using $N = 2, 4, 8, 12, 20$ number of terms in the sum, where $F_0 = 100, L = 80, H = 110, \theta = 0.02, a = 626, \mu = 0.1, \rho = 0.0001, t = 0.01$. As shown in

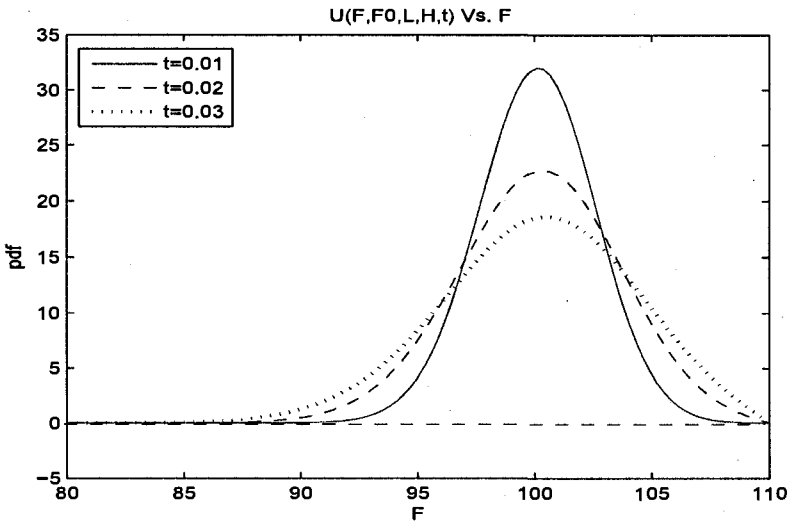


Figure 2.4.2: Converged p.d.f.s.

the figure, equation (2.4.1) gives a rapidly convergent series expansion for $U(F, F_0, L, H, t)$.

Figure 2.4.2 shows the (converged) transition densities $U(F, F_0, L, H, t)$ with different values of $t$ and fixed parameters $F_0 = 100, L = 80, H = 110, \theta = 0.02, a = 626, \mu = 0.1$ and $\rho = 0.0001$.

Single-barrier transition probability densities, for either upper or lower barrier, are obtained by a similar direct substitution as in the double-barrier case, i.e. substitute $\hat{u}(x, \rho)$, defined in equation (2.3.3), and a probability density $u(x, x_0, x_L, t)$ (for lower barrier) or $u(x, x_0, x_H, t)$ (for upper barrier) into equation (2.1.11). On the other hand, we can obtain single-barrier densities by a limiting approach. That is, taking $L \to 0+$ of the double barrier p.d.f, $U(F, F_0, L, H, t)$, leads to an upper barrier p.d.f. and the limit $H \to \infty$ of $U(F, F_0, L, H, t)$ gives the single lower barrier transition p.d.f.

Similarly, the transition probability densities of a four-parameter Bessel $I$-subfamily, can be achieved by directly substituting equation (2.3.4) into (2.1.11). In this thesis we only consider the Bessel $K$-subfamily. The main reason for this is that the "discounted" process $(e^{-\theta t}\mathrm{F}_t)_{t\geq 0} \in (0,\infty)$ is a martingale for all choices of parameters, which is crucial for applications in arbitrage-free option pricing. On the other hand, the Bessel $I$-subfamily of discounted process on $(0,\infty)$ are strict supermartingales. For detailed analysis of properties of these processes see Campolieti G. and Makarov R., 2006; 2008.

CHAPTER 3

# Pricing Formulas For F-Diffusions

In this chapter, we derive analytical pricing formulas for European barrier options under the drifted Bessel $K$-family of diffusions. A barrier option is a type of option contract where the option value depends on whether the underlying asset crosses a given barrier level, either from above or below. In what follows we deal explicitly with knock-out barriers. The pricing of the corresponding knock-in barrier options follows immediately by knock-in/knock-out symmetry.

Suppose the price of an asset (e.g. a stock) at calendar time $t$ is given by the process $(\mathrm{F}_t)_{t\geq 0}$ and hence obeys the stochastic differential equation

$$d\mathrm{F}_t = r\mathrm{F}_t dt + \sigma(\mathrm{F}_t)dW_t,\ \mathrm{F}_0 = F_0 \tag{3.0.3}$$

where $\mathrm{F}_t$ is a drifted Bessel-$K$ diffusion with volatility in (2.3.3). $W_t$ is a standard Brownian motion within an assumed risk-neutral measure where $(e^{-rt}\mathrm{F}_t)_{t\geq 0}$ is a martingale.

To simplify notation, and without loss in generality, we set current time as $t = 0$. Throughout we will use the following representations:

- $T > 0$ represents the time to maturity.
- $\mathrm{F}_T$ represents the underlying asset price at maturity time $T$.
- $F_0$ represents the current (spot) price of the underlying asset.
- $K > 0$ represents the strike or exercise price.
- $r$ represents the continuously compounded annual interest rate.

- $L > 0$ represents the lower barrier.
- $H > L$ represents the upper barrier.

Recall the payoff of a standard European option, denoted by $\Lambda(F_T)$, given as

$$\Lambda(\mathrm{F}_T) = \begin{cases} \max[(\mathrm{F}_T - K), 0] = (\mathrm{F}_T - K)^+, & \text{for call option;} \\ \max[(K - \mathrm{F}_T), 0] = (K - \mathrm{F}_T)^+, & \text{for put option.} \end{cases} \tag{3.0.4}$$

We denote a double-barrier payoff function by $\Lambda^{(L,H)}$, where $L$ and $H$ are lower and upper barriers, respectively. We assume $\Lambda(\cdot) \in L^2(S, m_\rho)$, where $S$ is the regular state space of the $F$-diffusion.

Now, consider the possibilities that the process $\mathrm{F}_t$ might cross lower barrier $L$ or upper barrier $H$. That is, if $\mathrm{F}_t$ crosses level $L$, the option contract is knocked-out (i.e. canceled and has zero value). Similarly, if the process $\mathrm{F}_t$ reaches an upper barrier $H$, the option contract is knocked-out, and hence, in either case the payoff $\Lambda^{(L,H)}(\mathrm{F}_T) = 0$. Otherwise, the process $\mathrm{F}_T \in (L, H)$ (i.e. $\tau_L, \tau_H > T$) and the double-barrier payoff $\Lambda^{(L,H)}(\mathrm{F}_T) = \Lambda(\mathrm{F}_T)$, as shown in Figure 3.0.1. Therefore, we define a double-barrier payoff, $\Lambda^{(L,H)}$, as follows:

$$\Lambda^{(L,H)}(\mathrm{F}_T) = \begin{cases} 0, & \tau_L \leq T \text{ or } \tau_H \leq T; \\ \Lambda(\mathrm{F}_T), & \tau_L, \tau_H > T; \end{cases} \tag{3.0.5}$$

Similarly, we denote the upper barrier knock-out payoff function by $\Lambda^{(H)}$. If the process $\mathrm{F}_t$ crosses an upper barrier $H$ ($\tau_H \leq T$), then the option contract is knocked-out. This means that the payoff $\Lambda^{(H)}(\mathrm{F}_T) = 0$. On the other hand, if the process $\mathrm{F}_t$ reaches 0 (or $T \geq \tau_0$), we have two possible cases. Case one: for a call payoff, $\Lambda^{(H)}(\mathrm{F}_T) = \Lambda(0) = (0 - K)^+ = 0$. Case

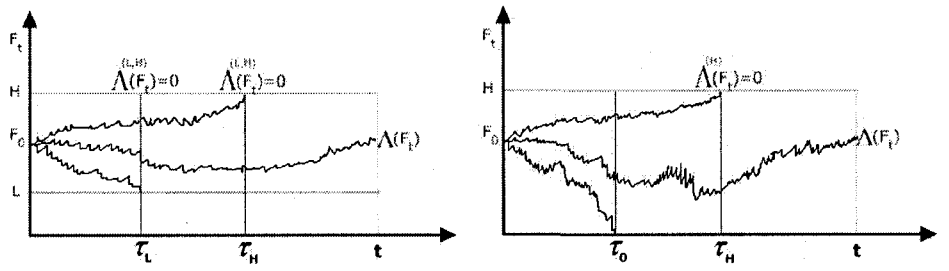


Figure 3.0.1: Typical double barrier payoff ( note $t = T$).

two: for a put payoff, $\Lambda^{(H)}(\mathrm{F}_T) = \Lambda(0) = (K-0)^+ = K$. The payoffs for the different possible scenarios are depicted in Figure 3.0.1. Therefore we define $\Lambda^{(H)}(\mathrm{F}_T)$ as

$$\Lambda^{(H)}(\mathrm{F}_T) = \begin{cases} \begin{cases} K, & \text{for put;} \\ 0, & \text{for call.} \end{cases}, & \tau_0 \leq T, \tau_0 < \tau_H; \\ \Lambda(\mathrm{F}_T), & \tau_0, \tau_H > T; \\ 0, & \tau_H \leq T, \tau_H < \tau_0. \end{cases} \tag{3.0.6}$$

Note that the above put payoff points to yet another important difference between the Bessel-$K$ model and the standard GBM model of Black-Scholes theory. When asset prices are assumed to obey the GBM process then no default scenarios are possible since the origin is a natural boundary and is hence not attainable in finite time. In contrast, if asset prices are modeled according to the drifted Bessel-$K$ diffusion then the origin is an exit boundary (i.e. attainable). In this case we tacitly assume the process stays at zero. The latter gives an asset pricing model that admits the possibility of default and, within the default scenario, the asset price hits zero in finite time with put payoff having maximal nonzero value of $K$.

For a single lower barrier the payoff is denoted by $\Lambda^{(L)}$. If $\mathrm{F}_t$ hits a lower barrier $L$ ($\tau_L \leq T$), the option contract is knocked-out and hence the payoff is $\Lambda^{(L)}(\mathrm{F}_t) = 0$ and if $\tau_L > T$ the payoff is $\Lambda^{(L)}(\mathrm{F}_T) = \Lambda(\mathrm{F}_T)$. Therefore

$$\Lambda^{(L)}(\mathrm{F}_T) = \begin{cases} \Lambda(\mathrm{F}_T), & \tau_L > T; \\ 0, & \tau_L \leq T. \end{cases} \tag{3.0.7}$$

The double-barrier pricing formulas for F-diffusions can be obtained via the *risk-neutral probability measure*, denoted by $\mathbb{P}$, with probability density function $U(F, F_0, L, H, t)$. In particular, the present value of the double-barrier option is given by the conditional expectation of the discounted payoff under the $\mathbb{P}$-measure:

$$V^{DB}(F, F_0, T) = e^{-rt}\mathbb{E}\left[\Lambda^{(L,H)}(\mathrm{F}_T)|\mathrm{F}_0 = F_0\right] \tag{3.0.8}$$

We note that the discounted asset price process, modeled as a drifted Bessel-$K$ process with $\theta = r$, where $r$ is the constant interest rate, is a $\mathbb{P}$-martingale.

The single knock-out barrier pricing formulas, either upper or lower, are achieved by replacing $\Lambda^{(L,H)}$ with $\Lambda^{(L)}$ or $\Lambda^{(H)}$ in equation (3.0.8). Another method for obtaining the single-barrier pricing formulas is by using the limiting approach. That is, letting $L \to 0+$ in (3.0.8) leads to an upper barrier pricing formula. Similarly, $\lim_{H\to\infty} V^{DB}(F, F_0, t)$ gives a single lower barrier pricing formula. Later in this chapter, we use this method to derive up-and-out and down-and-out call, and up-and-out put pricing formulas.

Before we derive the European double barrier (i.e. double knock-out) pricing formulas using equation (3.0.8), it is convenient if we first compute a cumulative transition distribution, denoted by $\Phi(F, F_0, t)$, and a related cumulative transition distribution, denoted as $\overline{\Phi}(F, F_0, t)$.

From the transition probability density, $U(F, F_0, L, H, t)$, given in equation (2.4.1), we define a cumulative probability distribution by

$$\Phi(F, F_0, t) := \int_L^F U(\overline{F}, F_0, L, H, t) d\overline{F}, \tag{3.0.9}$$

$F, F_0 \in [L, H]$. This integral is readily computed by changing integration variable from $\overline{F}$ to $x$. This can be done by the map $\overline{F} = \mathsf{F}(x)$, with inverse $x = \mathsf{X}(\overline{F})$, $d\overline{F} = \mathsf{F}'(x)dx$, $|\mathsf{F}'(x)| = \nu(x)/\sigma(\overline{F})$, giving

$$\Phi(F, F_0, t) = \int_{\mathsf{X}(L)}^{\mathsf{X}(F)} |\mathsf{F}'(x)| U(\mathsf{F}(x), F_0, L, H, t) dx \tag{3.0.10}$$

Now, we substitute $U(F, F_0, L, H, t)$, given in equation (2.4.1), into equation (3.0.10) and simplify giving the spectral expansion

$$\Phi(F, F_0, t) = \frac{1/2}{K_\mu(\sqrt{2\rho x_0})} \sum_{n=1}^{\infty} e^{-(\rho+\lambda_n)t} \mathcal{N}_n f_\mu(x_0, x_L, \lambda_n) \Psi_{n,\rho}(x), \tag{3.0.11}$$

where $x_L = \mathsf{X}(L), x_0 = \mathsf{X}(F_0), x = \mathsf{X}(F)$ and $\mathsf{X} = \mathsf{F}^{-1}$ is the inverse map for the Bessel-$K$ defined in (2.3.3). Throughout we define $\Psi_{n,\rho}$ as

$$\Psi_{n,\rho}(z) = \mathcal{N}_n \int_{\mathsf{X}(L)}^{z} K_\mu(\sqrt{2\rho x}) f_\mu(x, \mathsf{X}(L), \lambda_n) dx \tag{3.0.12}$$

The integral in (3.0.12) can be evaluated in closed-form as follows. Using the cylinder function $f_\mu(x, x_L, \lambda_n)$ of equation (1.2.6) and changing integration variable we have

$$\begin{aligned}\Psi_{n,\rho}(\mathsf{X}(F)) =& \mathcal{N}_n \int_{\mathsf{X}(L)}^{\mathsf{X}(F)} K_\mu(\sqrt{2\rho x})[J_\mu(\sqrt{2\lambda_n x_L})Y_\mu(\sqrt{2\lambda_n x}) \\ & - Y_\mu(\sqrt{2\lambda_n x_L})J_\mu(\sqrt{2\lambda_n x})]dx \\ =& 2\mathcal{N}_n J_\mu(\sqrt{2\lambda_n x_L}) \int_{\sqrt{\mathsf{X}(L)}}^{\sqrt{\mathsf{X}(F)}} x K_\mu(\sqrt{2\rho} x) Y_\mu(\sqrt{2\lambda_n} x) dx \\ & - 2\mathcal{N}_n Y_\mu(\sqrt{2\lambda_n x_L}) \int_{\sqrt{\mathsf{X}(L)}}^{\sqrt{\mathsf{X}(F)}} x K_\mu(\sqrt{2\rho} x) J_\mu(\sqrt{2\lambda_n} x) dx \end{aligned} \tag{3.0.13}$$

The last two integrals on the right can be computed by using the following indefinite integral identities (valid within an arbitrary constant):

$$\begin{aligned}\int x Y_\mu(ax) K_\mu(bx) dx &= \frac{x}{a^2+b^2}\left[aY_{\mu+1}(ax)K_\mu(bx) - bY_\mu(ax)K_{\mu+1}(bx)\right] \\ \int x J_\mu(ax) K_\mu(bx) dx &= \frac{x}{a^2+b^2}\left[aJ_{\mu+1}(ax)K_\mu(bx) - bJ_\mu(ax)K_{\mu+1}(bx)\right]\end{aligned}$$

Hence, after some algebra, equation (3.0.13) simplifies to

$$\begin{aligned}\Psi_{n,\rho}(x) = \frac{1}{\rho+\lambda_n}[&-\sqrt{2\lambda_n x} K_\mu(\sqrt{2\rho x})\,\widetilde{\phi}_n(x) \\ & - x^{\mu/2}\sqrt{2\rho x} K_{\mu+1}(\sqrt{2\rho x})\,\phi_n(x) + \frac{2}{\pi}\mathcal{N}_n K_\mu(\sqrt{2\rho x_L})],\end{aligned} \tag{3.0.14}$$

where $x = \mathsf{X}(F)$, $x_L = \mathsf{X}(L)$ and $\widetilde{\phi}_n(x)$ is given by an associated cylinder function

$$\widetilde{\phi}_n(x) = \mathcal{N}_n\left[Y_\mu(\sqrt{2\lambda_n x_L})J_{\mu+1}(\sqrt{2\lambda_n x}) - J_\mu(\sqrt{2\lambda_n x_L})Y_{\mu+1}(\sqrt{2\lambda_n x})\right] \tag{3.0.15}$$

Figure 3.0.2 contains plots of partial sums using (3.0.11) for $\Phi(F, F_0, t)$ with fixed values $F_0 = 100, L = 80, H = 110, r = 0.02, a = 626, \mu = 0.1, \rho =$

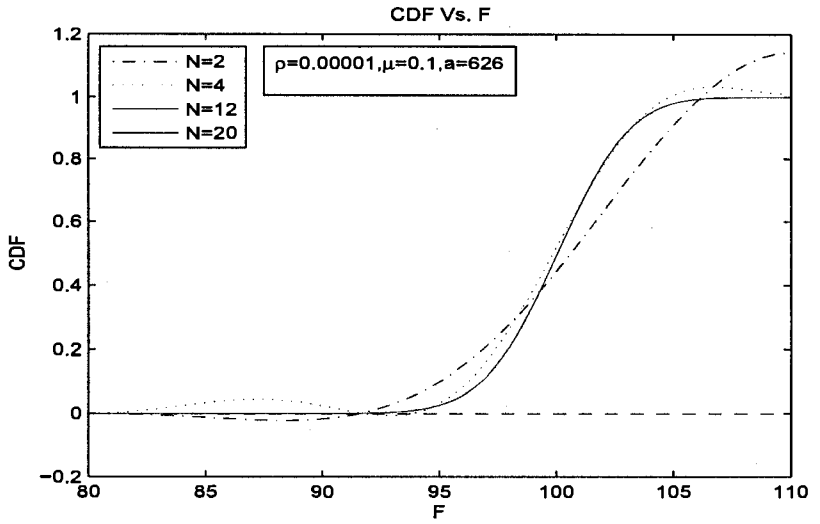


Figure 3.0.2: Rapid convergence of c.d.f.s.

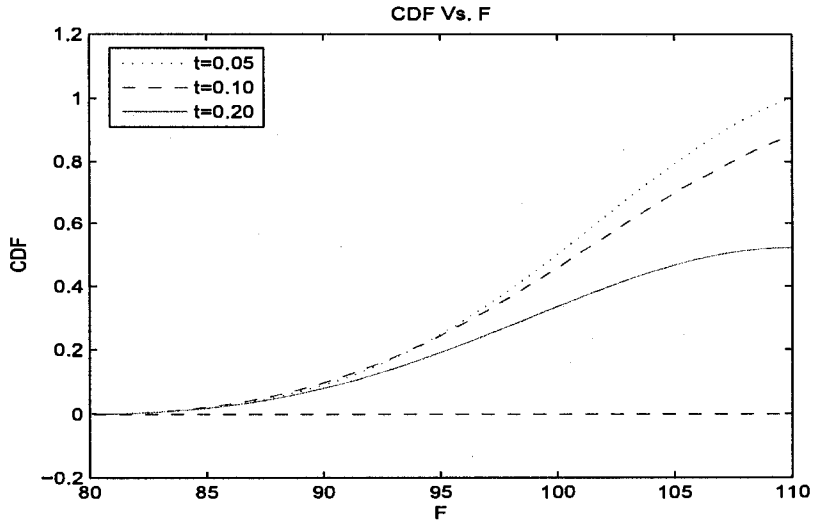


Figure 3.0.3: converged c.d.f.s.

$0.00001, t = 0.01$. We see that the spectral expansion in (3.0.11) is rapidly convergent as more terms are added to the series. The five different curves

correspond to the series sum in the first $N = 2, 4, 8, 12$ and 20 terms of the series in (3.0.11).

Figure 3.0.3 gives plots of numerically (converged) cumulative distributions in (3.0.11) with different values $t = 0.01, 0.05, 0.1$ and fixed parameters $F_0 = 100, L = 80, H = 110, r = 0.02, a = 626, \mu = 0.1$ and $\rho = 0.00001$.

Similarly, the related cumulative distribution $\overline{\Phi}(F, F_0, t)$ is defined as

$$\overline{\Phi}(F, F_0, t) := \int_{\mathsf{X}(L)}^{\mathsf{X}(F)} |\mathsf{F}'(x)| U(\mathsf{F}(x), F_0, L, H, t) \mathsf{F}(x) dx \tag{3.0.16}$$

The analogue to equation (3.0.11) is

$$\overline{\Phi}(F, F_0, t) = \frac{a/2}{K_\mu(\sqrt{2\rho x_0})} \sum_{n=1}^{\infty} e^{-(\rho+\lambda_n)t} \mathcal{N}_n f_\mu(x_0, x_L, \lambda_n) \overline{\Psi}_{n,\rho}(x), \tag{3.0.17}$$

where $\overline{\Psi}_{n,\rho}$ is defined as:

$$\overline{\Psi}_{n,\rho}(z) = \mathcal{N}_n \int_{x_L}^{z} I_\mu(\sqrt{2(\rho + r)x}) f_\mu(x, x_L, \lambda_n) dx \tag{3.0.18}$$

Using the cylinder function $f_\mu(x, x_L, \lambda_n)$ in equation (1.2.6) we have

$$\begin{aligned} \overline{\Psi}_{n,\rho}(\mathsf{X}(F)) = {} & 2\mathcal{N}_n J_\mu(\sqrt{2\lambda_n x_L}) \int_{\sqrt{\mathsf{X}(L)}}^{\sqrt{\mathsf{X}(F)}} x I_\mu(\sqrt{2(\rho + r)}x) Y_\mu(\sqrt{2\lambda_n}x) dx \\ & - 2\mathcal{N}_n Y_\mu(\sqrt{2\lambda_n x_L}) \int_{\sqrt{\mathsf{X}(L)}}^{\sqrt{\mathsf{X}(F)}} x I_\mu(\sqrt{2(\rho + r)}x) J_\mu(\sqrt{2\lambda_n}x) dx \end{aligned} \tag{3.0.19}$$

Similarly, we compute the integrals in equation (3.0.19) above by using the indefinite integral identities (valid within an arbitrary constant):

$$\begin{aligned}\int xY_\mu(ax)I_\mu(bx)dx &= \frac{x}{a^2+b^2}\left[bY_{\mu+1}(ax)I_\mu(bx)+aY_\mu(ax)I_{\mu+1}(bx)\right]\\ \int xJ_\mu(ax)I_\mu(bx)dx &= \frac{x}{a^2+b^2}\left[aJ_{\mu+1}(ax)I_\mu(bx)+bJ_\mu(ax)I_{\mu+1}(bx)\right]\end{aligned}$$

After simplification, the integrals in equation (3.0.19) reduce to the following compact form:

$$\begin{aligned}\overline{\Psi}_{n,\rho}(x) = \frac{1}{\rho+r+\lambda_n}\Big[&-\sqrt{2\lambda_n}xI_\mu(\sqrt{2(\rho+r)}x)\widetilde{\phi}_n(x)\\ &+x^{\mu/2}\sqrt{2(\rho+r)}xI_{\mu+1}(\sqrt{2(\rho+r)}x)\phi_n(x)+\frac{2}{\pi}\mathcal{N}_nI_\mu(\sqrt{2(\rho+r)}x_L)\Big]\end{aligned} \tag{3.0.20}$$

where $x=\mathsf{X}(F), x_L=\mathsf{X}(L), x_0=\mathsf{X}(F_0)$ are given by the inverse mapping for the Bessel $K$-subfamily defined in equation (2.3.3). $\widetilde{\phi}(x)$ is given in (3.0.15).

Figure 3.0.4 contains typical plots of partial sums using (3.0.17), where the parameters $F_0=100, L=80, H=110, r=0.02, a=626, \mu=0.1, \rho=0.00001, t=0.01$. Uniform rapid convergence is observed as more terms are added (i.e. $N=2,4,8,12,20$) in the series in (3.0.17).

Figure 3.0.5 displays some numerically plots of $\overline{\Phi}(F,F_0,t)$ given by equation (3.0.17) with constant parameters $F_0=100, L=80, H=110, r=0.02, a=626, \mu=0.1, \rho=0.00001$ and various times $t=0.01, 0.05, 0.1$.

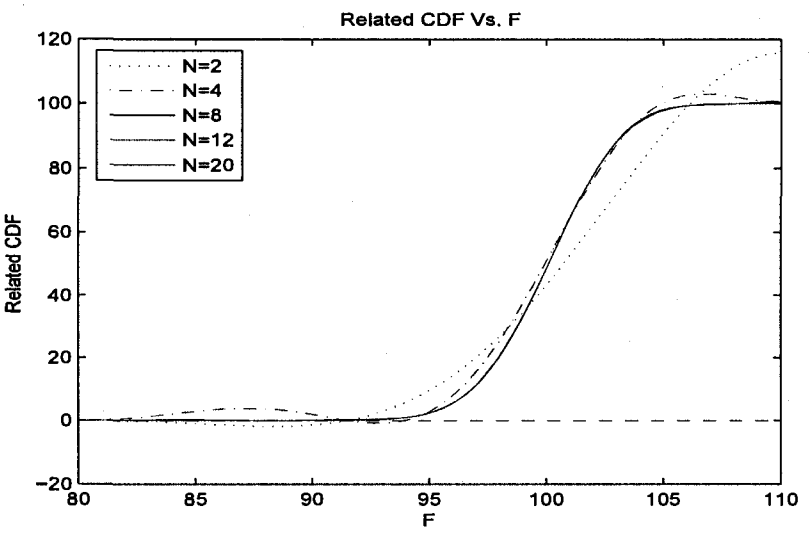


Figure 3.0.4: Rapid convergence of related c.d.f.s.

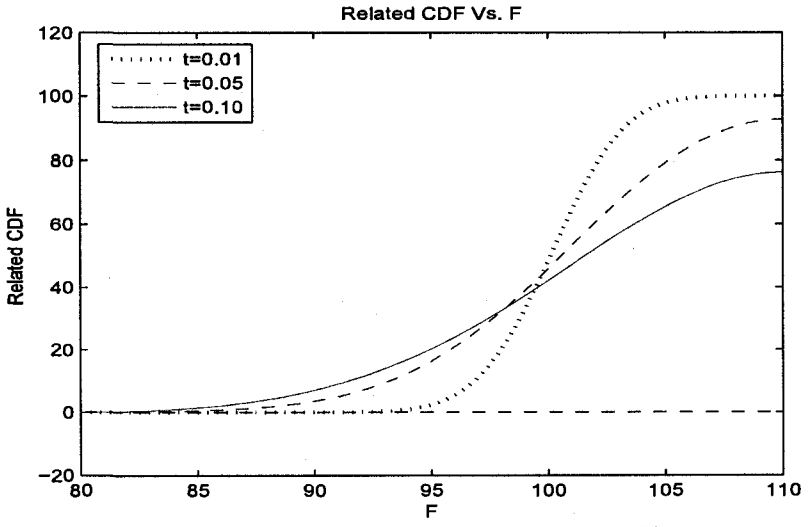


Figure 3.0.5: Converged related c.d.fs.

## 3.1. European Barrier Call Options

In this section, we derive pricing formulas for European barrier call options where the underlying asset follows a drifted Bessel-$K$ process. The derivations include double knock-out, down-and-out and up-and-out call options. The derivations follow by the risk-neutral pricing formula, given in (3.0.8). In what follows, we introduce the indicator set function, $\mathbb{1}_A(\omega)$, where $\mathbb{1}_A(\omega)$ is 1 for all $\omega \in A \subset \mathcal{F}_T$ and 0 otherwise. We implement the usual formalism of a filtered probability space whereby $\left(\mathcal{F}_t\right)_{0\leq t\leq T}$ is the natural filtration generated by the asset price diffusion process $(\mathrm{F}_t)_{0\leq t\leq T}$. The first hitting times $\tau_L$ and $\tau_H$ are defined in (2.2.2).

**3.1.1. Double-Knock-Out Call.** We now derive a double knock-out European call option value, denoted by $C(L, H, F_0, K, T)$, where $L$ and $H$ are lower and upper barrier levels, respectively. A double knock-out payoff function, $\Lambda^{(L,H)}$, is given in equation (3.0.5). Hence, it follows from the risk-neutral pricing formula (equation (3.0.8)) and equations (3.0.4), (3.0.5) that the double knock-out call with time-to-maturity $T$ has present value

$$C(L, H, F_0, K, T) = e^{-rT}\mathbb{E}\left[(\mathrm{F}_T - K)^+ \mathbb{1}_{\{\tau_H > T, \tau_L > T\}} | \mathrm{F}_0 = F_0\right] \qquad (3.1.1)$$

For $L \leq K \leq H$, the double knock-out call option value $C(L, H, F_0, K, T)$ is hence given by the integral over the (risk-neutral) transition p.d.f. for the

asset price process killed at both barriers:

$$\begin{aligned} C(L,H,F_0,K,T) &= e^{-rT}\int_L^H U(F,F_0,L,H,T)(F-K)^+dF \\ &= e^{-rT}\int_K^H U(F,F_0,L,H,T)FdF \\ &\quad - Ke^{-rT}\int_K^H U(F,F_0,L,H,T)dF \end{aligned} \tag{3.1.2}$$

where $U(F,F_0,L,H,T)$ is given in equation (2.4.1). Using the definition of $\Phi(F,F_0,t)$, with spectral expansion given in (3.0.11), and of $\overline{\Phi}(F,F_0,t)$ given by (3.0.17), the European double knock-out call option has value

$$\begin{aligned} C(L,H,F_0,K,T) &= e^{-rT}[\overline{\Phi}(H,F_0,T) - \overline{\Phi}(K,F_0,T)] \\ &\quad - e^{-rT}K\left[\Phi(H,F_0,T) - \Phi(K,F_0,T)\right] \end{aligned} \tag{3.1.3}$$

Numerical results for the valuation of double knock-out using (3.1.3) are presented in Figures (3.1.1)-(3.1.4).

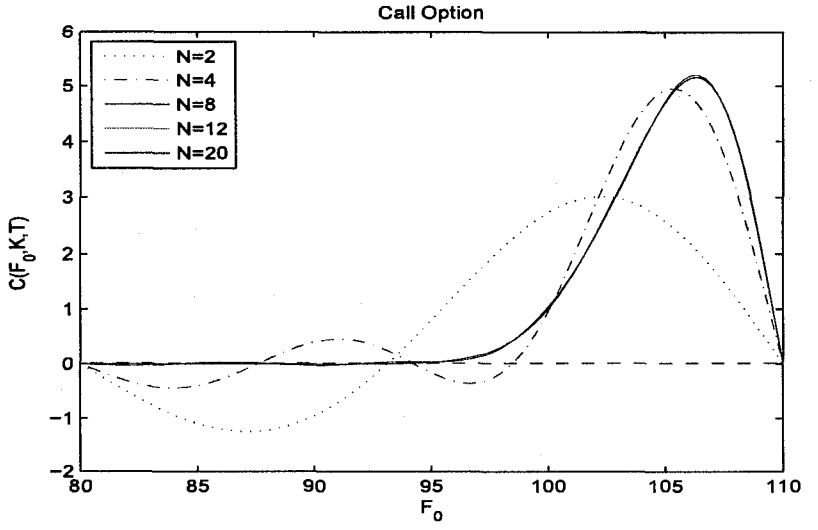


Figure 3.1.1: Rapid convergence of double knock-out call series expansion.

Figure 3.1.1 shows plots of partial sums for the series in (3.1.3) for the double knock-out European call option value as function of spot price $F_0$, with fixed parameters $L = 80, H = 110, r = 0.02, \rho = 0.00001, \mu = 0.1, a = 626, t = 0.01$ and $K = 100$. As shown, the double knock-out call series converges rapidly as more terms are included. The five distinct curves represent the series sum in the first $N = 2, 4, 8, 12$ and 20 terms in the spectral expansion of $C(L, H, F_0, K, T)$.

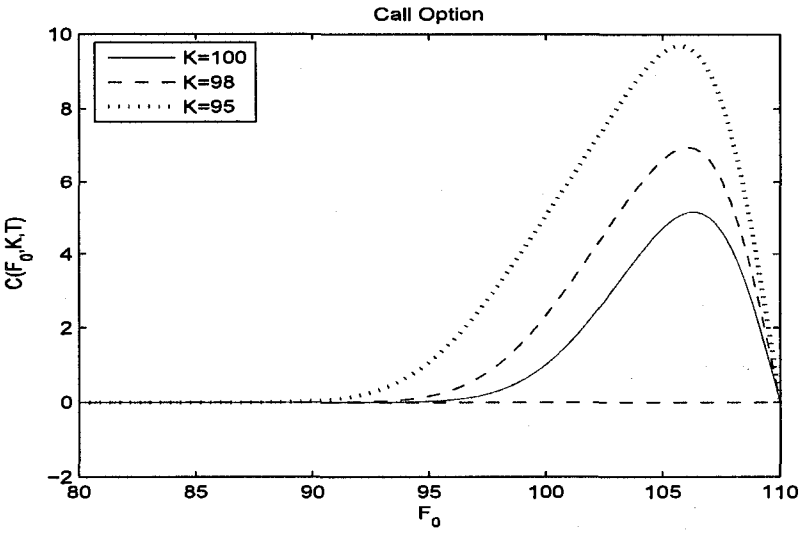


Figure 3.1.2: Converged double knock-out call.

Figure 3.1.2 shows plots (converged) of the double knock-out European call option values, with different choices of strike prices $K$ and fixed parameters $L = 80, H = 110, r = 0.02, \rho = 0.0001, \mu = 0.1, a = 626, T = 0.01$. As displayed in the figure, we notice that, as strike price $K$ increases, the option price values are shifted to the right. This is consistent with a greater probability for paths having terminal values $F_T > K$ as $F_0$ increases.

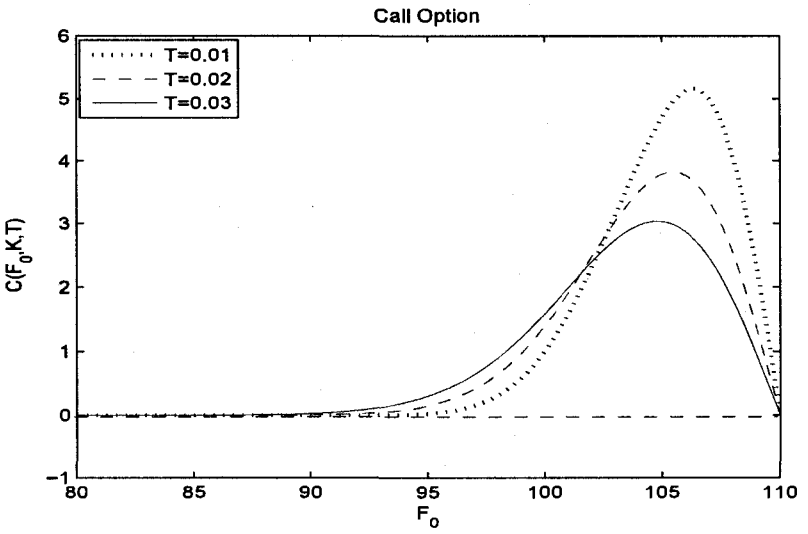


Figure 3.1.3: Converged double knock-out call option value.

Figure 3.1.3 gives plots of the double knock-out call value $C(L, H, F_0, K, T)$ as a function of spot $F_0$, with different time to maturities $T$ and fixed parameters $L = 20, H = 110, r = 0.02, \rho = 0.0001, \mu = 0.1, a = 626, K = 100$.

Converged plots of $C(L, H, F_0, K, T)$ are presented in Figure (3.1.4) with fixed $L = 80, H = 110, r = 0.02, \rho = 0.0001, T = 0.03, K = 100$ and various choices of $(\mu, a)$ in the Bessel-$K$ family. Note that the family with $\mu = 0.1$ corresponds to the local volatility with greatest steepness and highest leverage effect for a given spot price $F_0$.

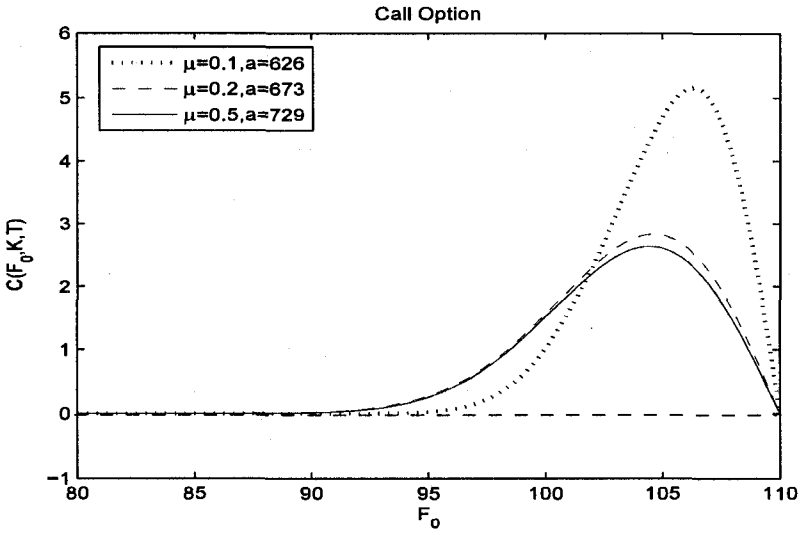


Figure 3.1.4: Converged double knock-out call value.

For strike price $K$ below both barriers (i.e. $K \leq L \leq H$), the European double knock-out call option value, $C(L, H, F_0, K, T)$, is given by

$$\begin{aligned} C(L,H,F_0,K,T) &= e^{-rT}\int_L^H U(F,F_0,L,H,T)(F-K)^+dF \\ &= e^{-rT}\int_L^H U(F,F_0,L,H,T)FdF \\ &\quad - e^{-rT}K\int_L^H U(F,F_0,L,H,T)dF \end{aligned} \tag{3.1.4}$$

with $U(F, F_0, L, H, T)$ given in equation (2.4.1). Using $\Phi(F, F_0, t)$, given in (3.0.11), and the related cumulative density, $\overline{\Phi}(F, F_0, t)$, given in (3.0.17), equation (3.1.4) leads to the following result:

$$C(L,H,F_0,K,T) = e^{-rT}[\overline{\Phi}(H,F_0,T) - K\Phi(H,F_0,T)] \tag{3.1.5}$$

Figure 3.1.5 gives plots of the double knock-out call value $C(L, H, F_0, K, T)$ (using equation (3.1.5)), as function of spot $F_0$ with fixed parameters $L =$

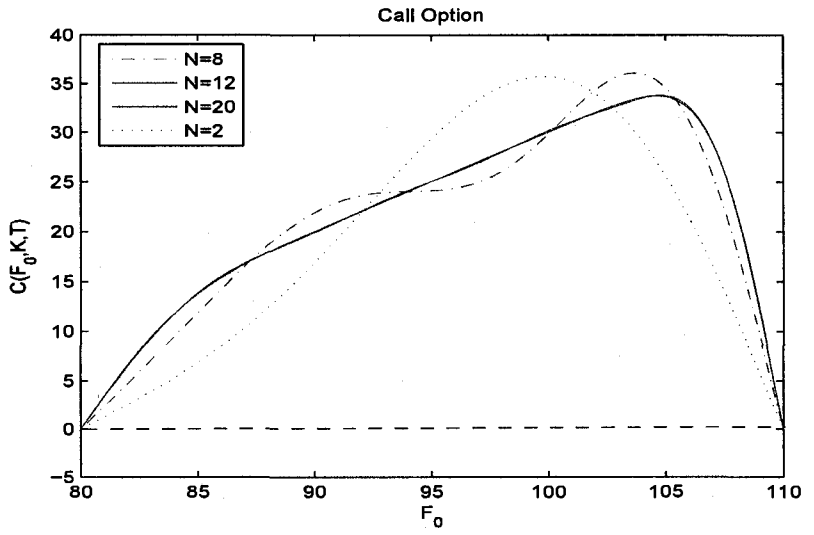


Figure 3.1.5: Convergence of spectral expansion for double knock-out call.

$80, H = 110, r = 0.02, a = 626, \mu = 0.01, \rho = 0.0001, K = 70, T = 0.01$. This figure shows the rapid convergence of the double knock-out call value $C(L, H, F_0, K, T)$, as more terms are included in the series sum in equation (3.1.5). The four distinct graphs correspond to the first $2, 8, 12$ and $20$ terms in the series for $C(L, H, F_0, K, T)$.

Figure 3.1.6 shows converged double knock-out call values using equation (3.1.5) with different strike prices $K < L < H$, where $L = 80, H = 110, r = 0.02, a = 626, \mu = 0.1, \rho = 0.0001, T = 0.01$.

Figure 3.1.7 gives plots of converged double knock-out call values as function of spot $F_0$ for different values of $T$ and fixed parameters $L = 80, H = 110, r = 0.02, a = 626, \mu = 0.1, \rho = 0.0001, K = 70$.

Plots of the double knock-out call option values for $K < L < H$ are given in Figure 3.1.8. The three distinct curves represent the three choices of parameters $(\mu, a)$ with fixed value $L = 80, H = 110, r = 0.02, \rho = 0.0001, T =$

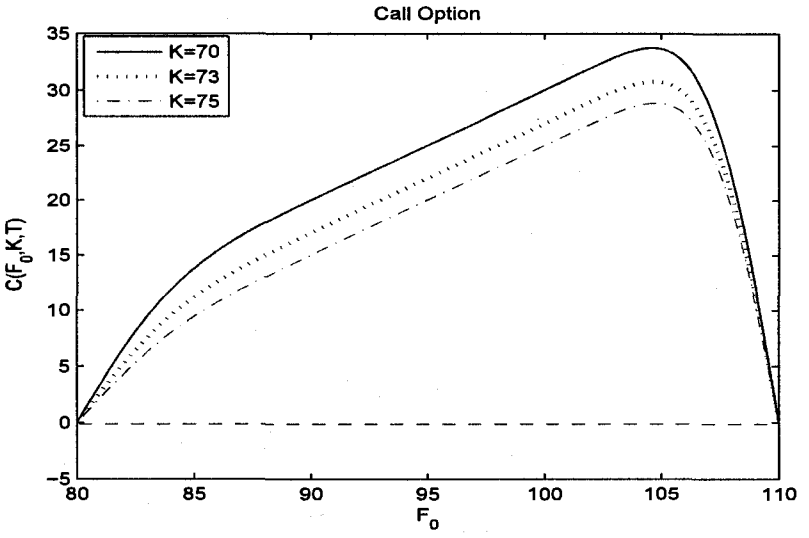


Figure 3.1.6: Converged double knock-out call value where $K < L < H$.

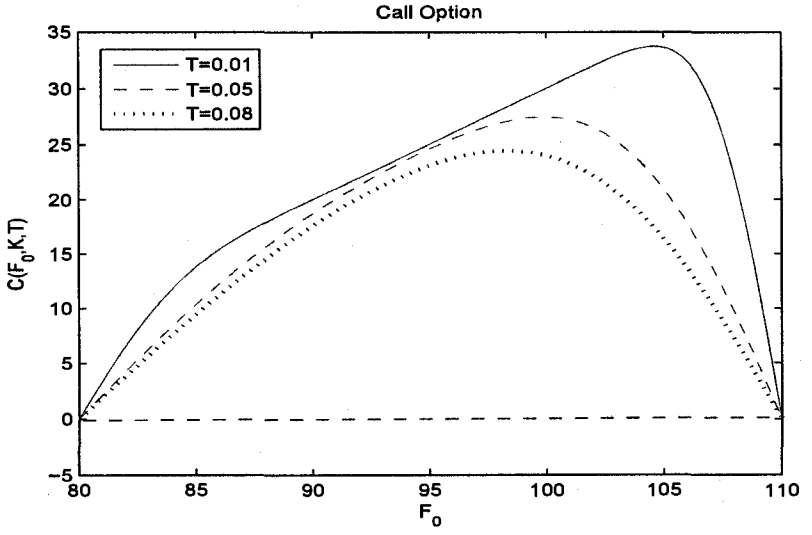


Figure 3.1.7: Converged double knock-out call value.

$0.01, K = 70$. The three sets of parameter choices for $(\mu, a)$ correspond to the respective local volatility curves in Figure 2.3.1. Note that smaller $\mu$

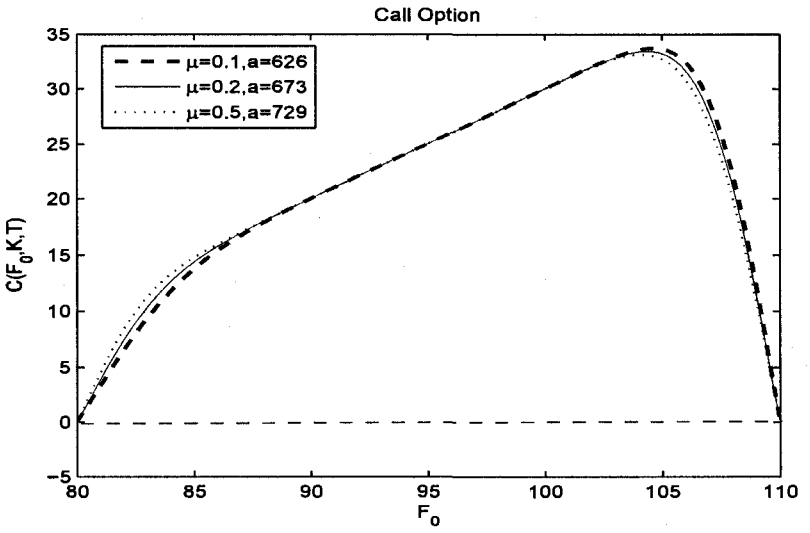


Figure 3.1.8: Converged double knock-out call values with $K < L < H$.

values correspond to steeper local volatility curves. The steepening of the local volatility has pronounced effects on the barrier option value at the extremities of the spot value $F_0$ close to either barrier $L$ or $H$.

**3.1.2. Down-and-out Call.** In this subsection we develop a pricing formula for a down-and-out European call option, which we denote by $C^{DO}(L, F_0, K, T)$, with $L > 0$ as a lower barrier. The derivation is obtained by using a limiting approach. That is, by taking limit $H \to \infty$ of the double knock-out call option value.

By risk-neutral pricing we have

$$\begin{aligned} C^{DO}(L, F_0, K, T) &= e^{-rT}\mathbb{E}[\Lambda^{(L)}(\mathrm{F}_T)|\mathrm{F}_0 = F_0] \\ &= e^{-rT}\mathbb{E}[(\mathrm{F}_T - K)^+ \mathbb{1}_{\{\tau_L > T\}}|\mathrm{F}_0 = F_0] \end{aligned} \tag{3.1.6}$$

where $\tau_L$ is given in equation (2.2.2). Note that, an indicator function in the last step of (3.1.6) can be rewritten as $\mathbb{1}_{\{\tau_L > T\}} = \lim_{H\to\infty} \mathbb{1}_{\{\tau_L > T, \tau_L < \tau_H\}}$.

Hence, equation (3.1.6) leads to:

$$\begin{aligned} C^{DO}(L, F_0, K, T) &= e^{-rT} \lim_{H\to\infty} E[(\mathrm{F}_T - K)^+ \mathbb{1}_{\{\tau_L > T, \tau_L < \tau_H\}} | \mathrm{F}_0 = F_0] \\ &= \lim_{H\to\infty} C(L, H, F_0, K, T) \end{aligned} \tag{3.1.7}$$

where $C(L, H, F_0, K, T)$ is the double knock-out call option value, given by equation (3.1.3) or (3.1.5).

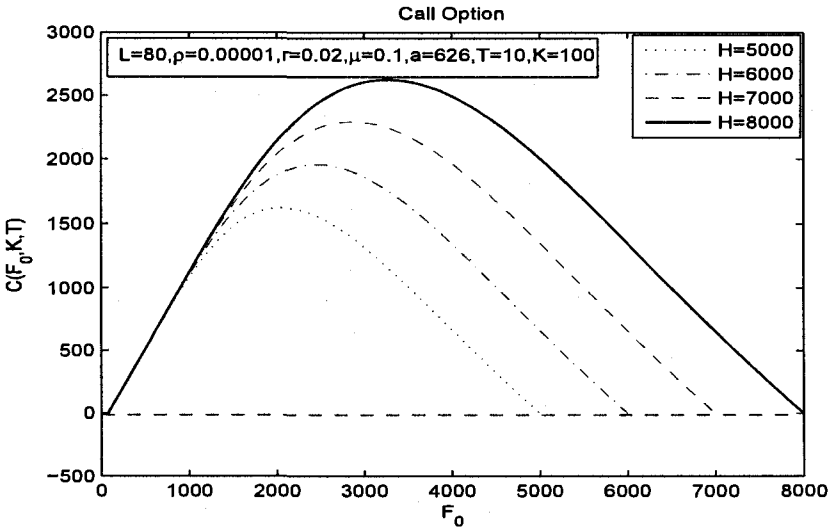


Figure 3.1.9: Convergence of down-and-out call value.

Figure 3.1.9 shows a sequence of double-barrier call values for increasing values of $H$, for $L = 80, r = 0.02, \rho = 0.0001, \mu = 0.1, a = 626, T = 10, K = 100, N = 150$. The graphs show the rapid convergence of the double-barrier values to the down-and-out call value within the region of interest for spot values on the order of $80 - 500$.

Figure 3.1.10 gives plots of down-and-out call values for three different families of Bessel-$K$ diffusions (i.e. three sets of $(\mu, a)$ values) and for the GBM model (thick solid line) with local volatility at spot $F_0 = 100$ chosen

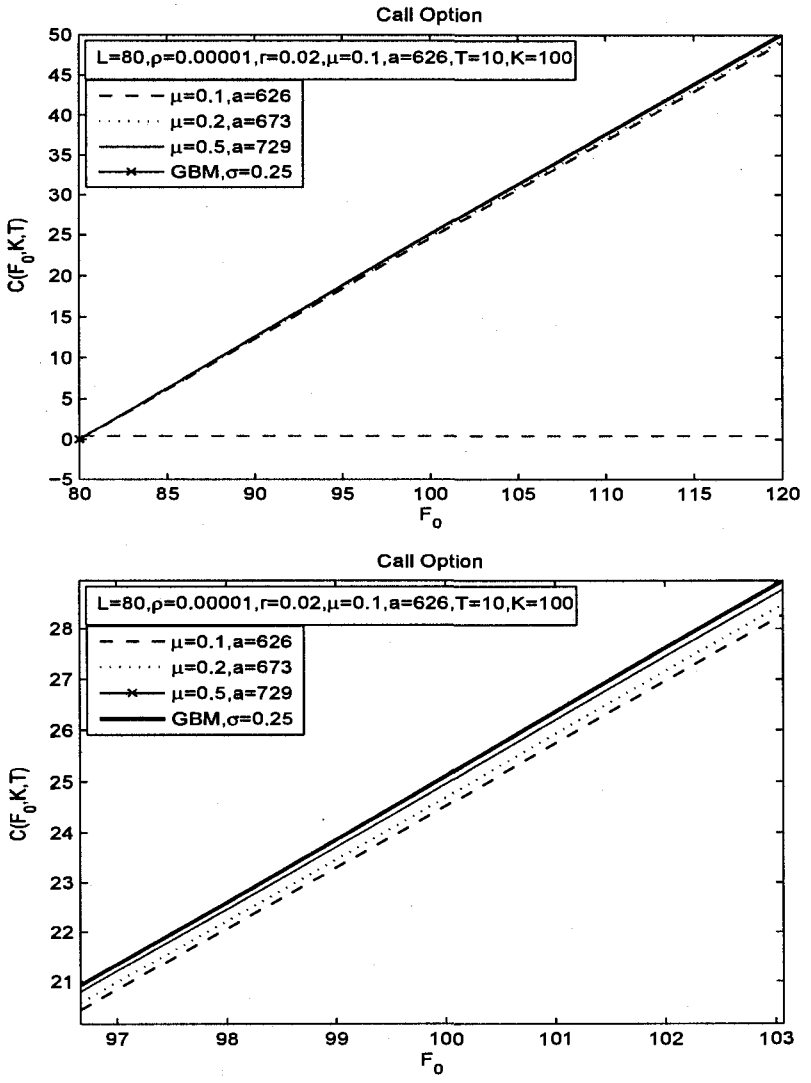


Figure 3.1.10: Converged down-and-out call in comparison with GBM model.

such that $\sigma(F_0)/F_0 = 0.25$, and fixed parameters $L = 80, r = 0.02, K = 100, T = 10$. As displayed, the three curves for the Bessel-$K$ model (with choices $(\mu, a)$) are quite close to the GBM model. On the other hand, the curve with $(\mu, a) = (0.5, 729)$ is much closer to the thick solid line

representing the GBM model than the other two sets of values $(\mu, a)$. This is consistent with the fact that the local volatility of the Bessel-$K$ model is flatter for larger $\mu$ values (approaching the GBM local volatility) for spot values $\gtrsim 100$. See Figure 2.3.1 for comparison.

**3.1.3. Up-and-out Call.** In this subsection we derive the pricing formula for an up-and-out European call, denoted by $C^{UO}(H, F_0, K, T)$, with upper barrier $H < \infty$. The derivations for an up-and-out call option are similar to that of the down-and-out call. However, we now consider the limit $L \to 0+$ of the double knock-out call value.

By risk-neutral pricing we have:

$$\begin{aligned} C^{UO}(H, F_0, K, T) &= e^{-rT}\mathbb{E}\left[\Lambda^{(H)}(\mathrm{F}_T)|\mathrm{F}_0 = F_0\right] \\ &= e^{-rT}\mathbb{E}\left[(\mathrm{F}_T - K)^+ \mathbb{1}_{\{\tau_0 > T\}}\mathbb{1}_{\{\tau_H > T\}}|\mathrm{F}_0 = F_0\right] \end{aligned} \tag{3.1.8}$$

where $\tau_L, \tau_H$ are defined in equation (2.2.2). The indicator functions can be rewritten as $\mathbb{1}_{\{\tau_0>T\}}\mathbb{1}_{\{\tau_H>T\}} = \mathbb{1}_{\{\tau_0>T,\tau_H>T\}} = \lim_{L\to 0+}\mathbb{1}_{\{\tau_L>T,\tau_H>T\}}$. Hence, equation (3.1.8) becomes:

$$\begin{aligned} C^{UO}(H, F_0, K, T) &= \lim_{L\to 0^+} e^{-rT}\mathbb{E}\left[(\mathrm{F}_T - K)^+ \mathbb{1}_{\{\tau_L>T,\tau_H>T\}}\middle|\, \mathrm{F}_0 = F_0\right] \\ &= \lim_{L\to 0^+} C(L, H, F_0, K, T) \end{aligned} \tag{3.1.9}$$

where $C(L, H, F_0, K, T)$ is the double knock-out call value.

Figure 3.1.11 shows the convergence of the limiting procedure as $L \to 0^+$ of $C(L, H, F_0, K, T)$ for $H = 300, r = 0.02, \rho = 0.00001, \mu = 0.1, a = 626, T = 10, K = 200, N = 100$. The double-barrier values $C(L, H, F_0, K, T)$ converge to $C^{UO}(H, F_0, K, T)$ as $L$ approaches zero (e.g. $L \approx 0.1$).

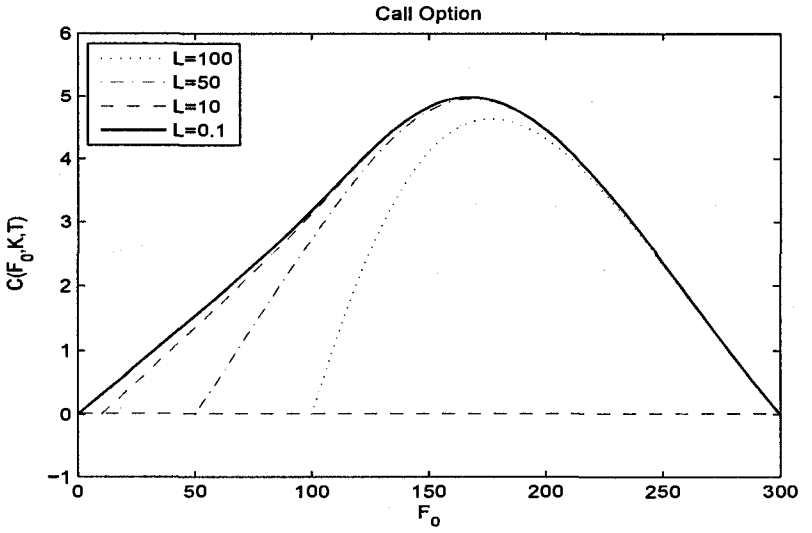


Figure 3.1.11: Convergence of double knock-out call to the up-and-out call.

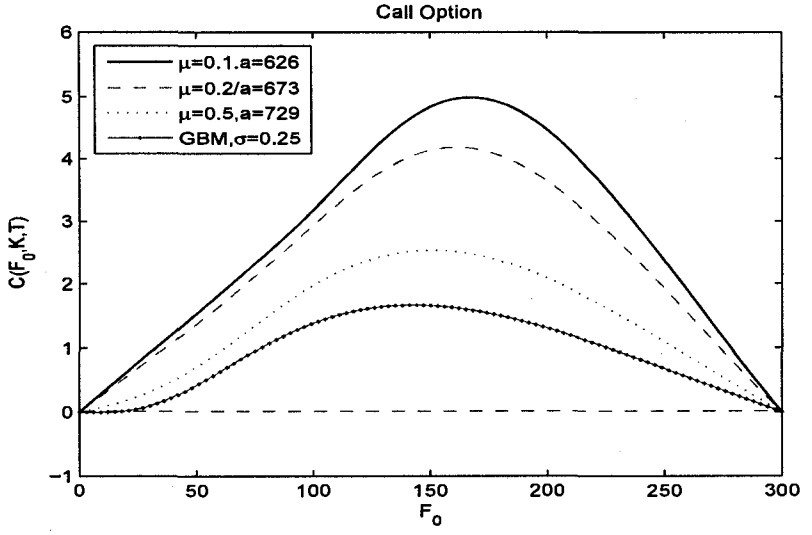


Figure 3.1.12: Converged up-and-out call in comparison with GBM model.

Figure 3.1.12 shows the converged up-and-out call values for three distinct sets of parameters $(\mu, a)$ (dotted lines) and an up-and-out GBM model

(solid dotted line), with local volatility $\sigma = 0.25$ at spot $F_0 = 100$, where $H = 300, r = 0.02, \rho = 0.00001, T = 10, K = 200$. The three graphs of $C^{UO}(H, F_0, K, t)$ for the Bessel-$K$ model (with choices of $(\mu, a)$) show quite different qualitative and quantitative behavior. The difference is pronounced for lower values of the spot $F_0 \lesssim 50$. For larger values of $\mu$, the Bessel-$K$ model is closer to the GBM model, whereas much steeper local volatility curves characterize the Bessel-$K$ model as $\mu \to 0+$. See Figure 2.3.1 for the comparison. The GBM model has constant local volatility and hence the call price approaches zero very rapidly as spot goes to zero. In contrast, the Bessel-$K$ diffusion exhibits a strong leverage effect for small values of the asset price. So the option price does not decrease sharply as spot $F_0 \to 0+$. This is particularly the case for smaller $\mu$ values, i.e. for Bessel-$K$ models with steeper local volatility profile. The Bessel-$K$ models also admit default, i.e. the asset price can hit zero in finite time as 0 is an exit boundary (see section 3.2.2 for details). This effect, in some sense, competes with the leverage effect to bring the call price down to zero as the spot $F_0 \to 0+$.

## 3.2. European Barrier Put Options

In this section, we derive the exact (closed-form spectral expansion) pricing formulas for European barrier put options for double knock-out and up-and-out put options. The derivations are similar to that of the barrier call options, except that the first hitting time at the origin now also plays a role. An up-and-out put option pricing formula can be derived via the above-mentioned limit approach. That is, by taking $L \to 0+$ of the double knock-out put option pricing formula.

**3.2.1. Double Knock-Out Put.** Let $P(L, H, F_0, K, T)$ denote the double knock-out put value, with lower barrier $L > 0$ and upper barrier $H > L$, spot price $F_0 \in [L, H]$ and time to maturity $T$. Following similar arguments in previous sections, the exact closed-form pricing formulas for double knock-out put options can be derived.

First we consider the case where the strike price $K$ is in between the barriers, i.e. $L \leq K \leq H$, then we have:

$$P(L, H, F_0, K, T) = e^{-rT}\mathbb{E}\left[(K - \mathrm{F}_T)^+ \mathbb{1}_{\{\tau_H > T, \tau_L > T\}} | \mathrm{F}_0 = F_0\right] \tag{3.2.1}$$

where $\tau_z$ is defined in equation (2.2.2).

The last expression in equation (3.2.1) can be computed by using the double-barrier transition probability density function $U$ of equation (2.4.1). Hence, equation (3.2.1) reduces to:

$$\begin{aligned} P(L, H, F_0, K, T) &= e^{-rT} \int_L^H U(F, F_0, L, H, t)(K - F)^+ dF \\ &= e^{-rT} K \int_L^K U(F, F_0, L, H, t) dF \\ &\quad - e^{-rT} \int_L^K U(F, F_0, L, H, t) F dF \end{aligned} \tag{3.2.2}$$

The integrals are computed by using the cumulative density $\Phi$ in equation (3.0.11) and the related cumulative density $\overline{\Phi}$ in equation (3.0.17). Combining gives an analytically exact spectral expansion for the double knock-out put value:

$$P(L, H, F_0, K, T) = e^{-rT}\left[K\Phi(K, F_0, T) - \overline{\Phi}(K, F_0, T)\right] \tag{3.2.3}$$

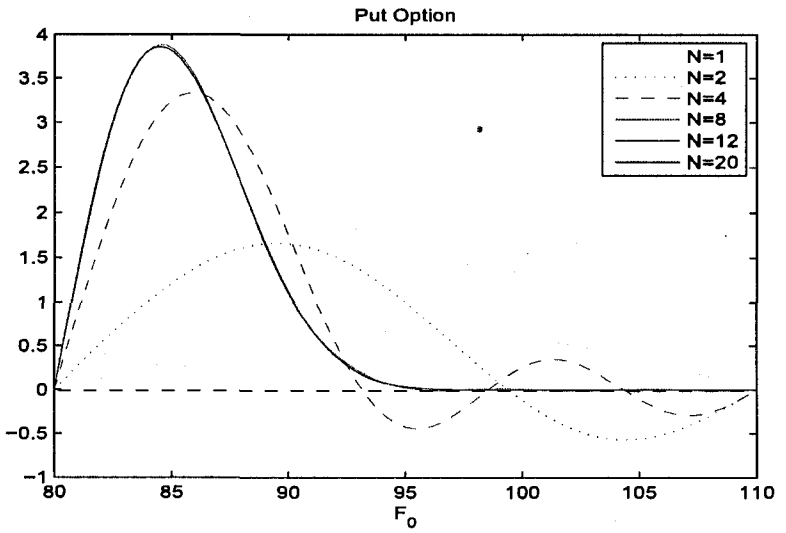


Figure 3.2.1: Rapid convergence of the spectral expansion for equation (3.2.3).

Figure 3.2.1 displays the convergence for the double knock-out European put option value using equation (3.2.3), as function of spot $F_0$, with fixed parameters $L = 80, H = 110, \rho = 0.00001, \mu = 0.1, r = 0.02, a = 626, T = 0.01, K = 90$. The six distinct curves correspond to the first $N = 1, 2, 4, 8, 12$ and 20 (solid line) terms of the series sum in equation (3.2.3).

Figure 3.2.2 contains some calculated curves for $P(L, H, F_0, K, T)$ using the spectral expansion in (3.2.3), were $L = 80, H = 110, \rho = 0.00001, \mu = 0.1, r = 0.02, a = 626, T = 0.01$ and different choices of strike price $K$.

Figure 3.2.3 shows curves for $P(L, H, F_0, K, T)$ for various $T$, where $L = 80, H = 110, \rho = 0.00001, \mu = 0.1, r = 0.02, a = 626, K = 90$.

Figure 3.2.4 displays curves for $P(L, H, F_0, K, T)$ for three choices of Bessel-$K$ models. The three curves correspond to the three separate sets

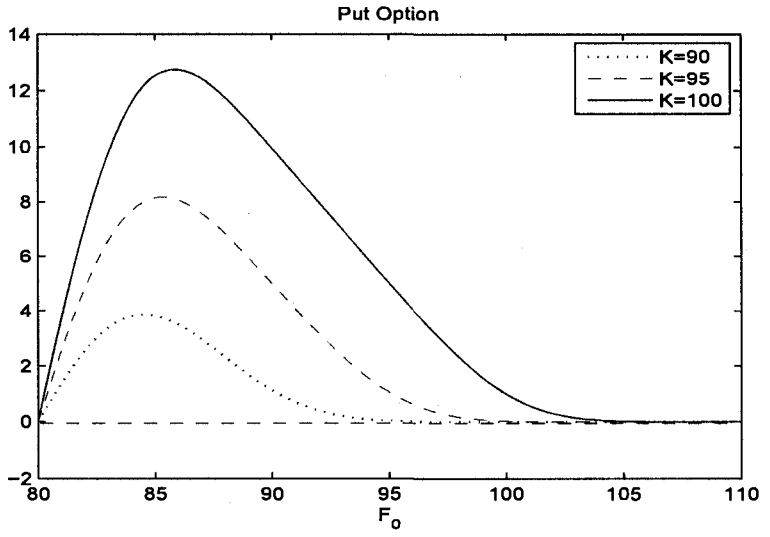


Figure 3.2.2: Converged double knock-out put values with various $K$ values.

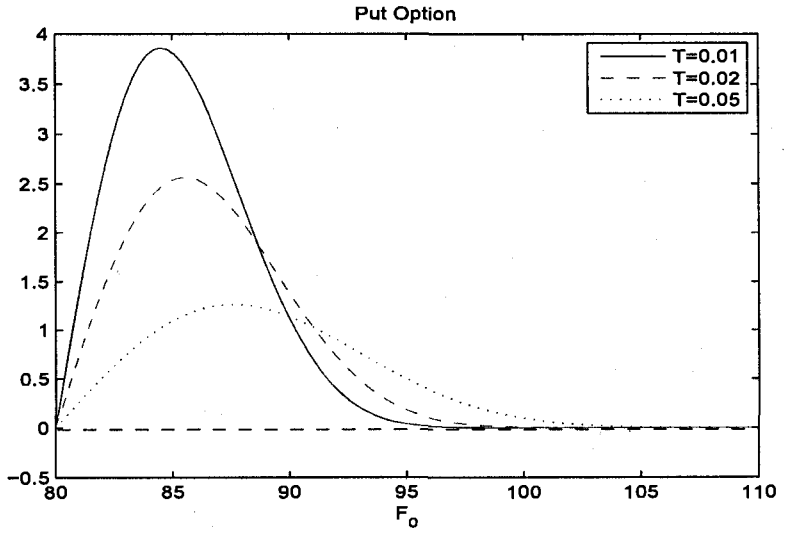


Figure 3.2.3: Converged double knock-out put value with various $T$.

of parameters $(\mu, a)$ as given in Figure 2.3.1, where $L = 80, H = 110, \rho = 0.00001, \theta = r = 0.02, T = 0.01, K = 90$.

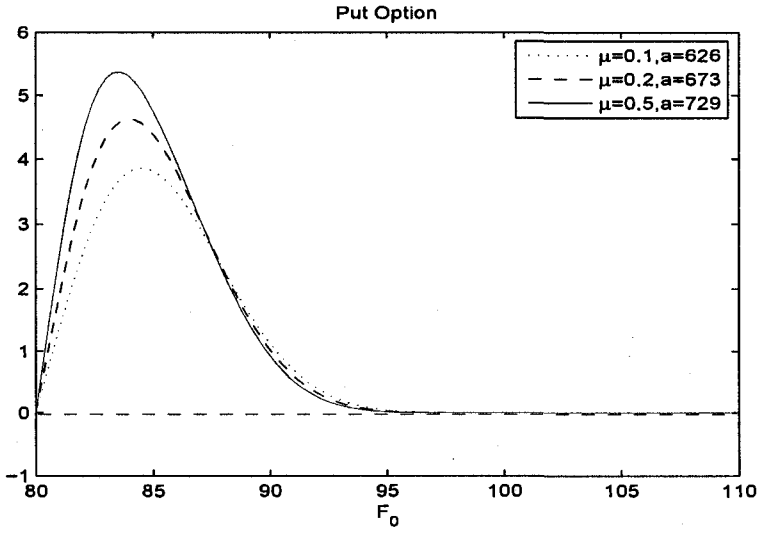


Figure 3.2.4: Converged double Knock-Out put for three sets of $(\mu, a)$.

Similarly, for the case where $L \leq H \leq K$, the double knock-out put option value is given by

$$\begin{aligned} P(L,H,F_0,K,T) &= e^{-rT}\mathbb{E}\left[(K-\mathrm{F}_T)^+ \mathbb{1}_{\{\tau_H>T,\tau_L>T\}} | \mathrm{F}_0 = F_0\right] \\ &= e^{-rT}\int_L^H U(F,F_0,L,H,T)(K-F)^+ dF \end{aligned} \tag{3.2.4}$$

where $U(F,F_0,L,H,T)$ is given in (2.4.1).

Using $\Phi(K,F_0,T)$ and $\overline{\Phi}(K,F_0,T)$ in equations (3.0.11) and (3.0.17), the double knock-out put option value is:

$$P(L,H,F_0,K,T) = e^{-rT}\left[K\Phi(H,F_0,T) - \overline{\Phi}(H,F_0,T)\right] \tag{3.2.5}$$

For the case that $K \leq L \leq H$, the value of the option $P(L,H,F_0,K,T)$ is trivially zero.

Figure 3.2.5 demonstrates the convergence of the spectral series for the put value given in equation (3.2.5), for all $F_0 \in [L,H]$ where $L = 80, H =$

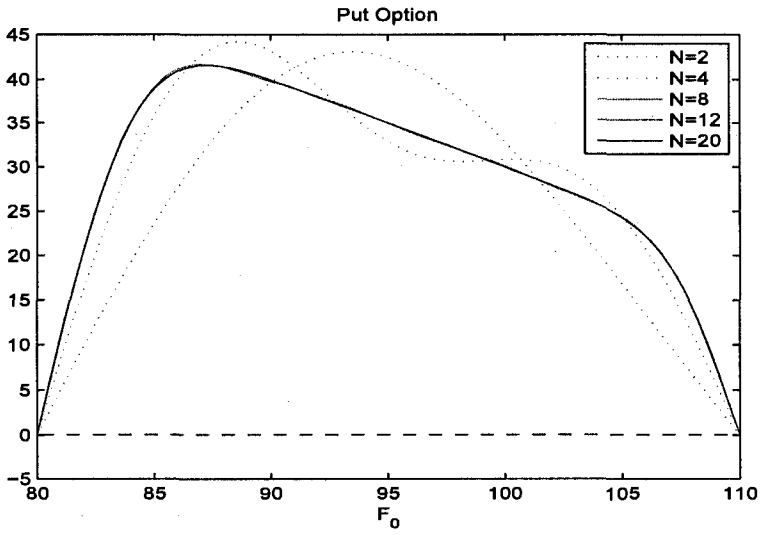


Figure 3.2.5: Series convergence for double knock-out put with $L \leq H \leq K$.

$110, \rho = 0.0001, \mu = 0.1, r = 0.02, a = 626, T = 0.01, K = 130$. As shown in the figure, the series converges quickly as more terms are added in the sum of equation (3.2.5). The five curves represent the series sum of the first $2, 4, 8, 12$ and $20$ (solid line) terms of the double knock-out put option formula.

Figure 3.2.6 displays the put value $P(L, H, F_0, K, T)$ using equation (3.2.5), as function of spot $F_0$, with fixed parameters $L = 80, H = 110, \rho = 0.00001, \mu = 0.1, r = 0.02, a = 626, T = 0.01$. The three curves correspond to the distinct choices of strike prices $K$ above the barriers.

Figure3.2.7 displays curves of $P(L, H, F_0, K, T)$ for various maturities with parameters $L = 80, H = 110, \rho = 0.00001, \mu = 0.1, r = 0.02, a = 626, K = 130$.

Figure 3.2.8 presents $P(L, H, F_0, K, T)$ for three choices of Bessel-$K$ diffusions where $L = 80, H = 110, \rho = 0.00001, r = 0.02, T = 0.01, K = 130$.

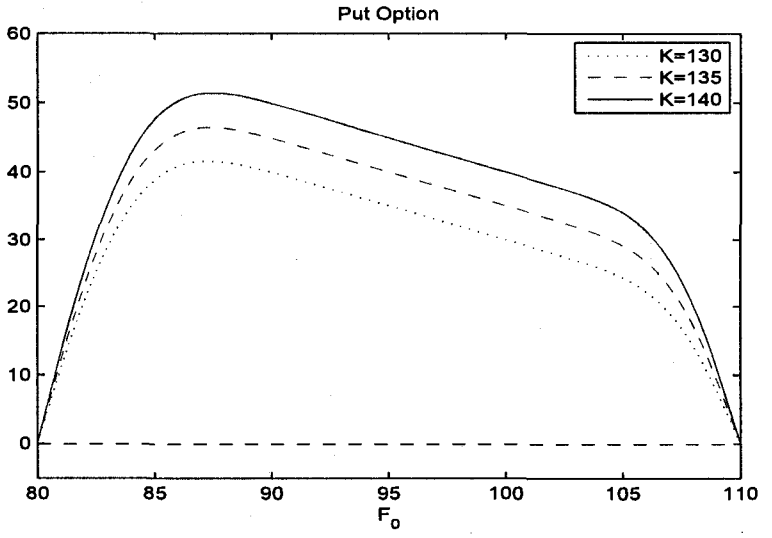


Figure 3.2.6: Converged double knock-out put option value for various $K$.

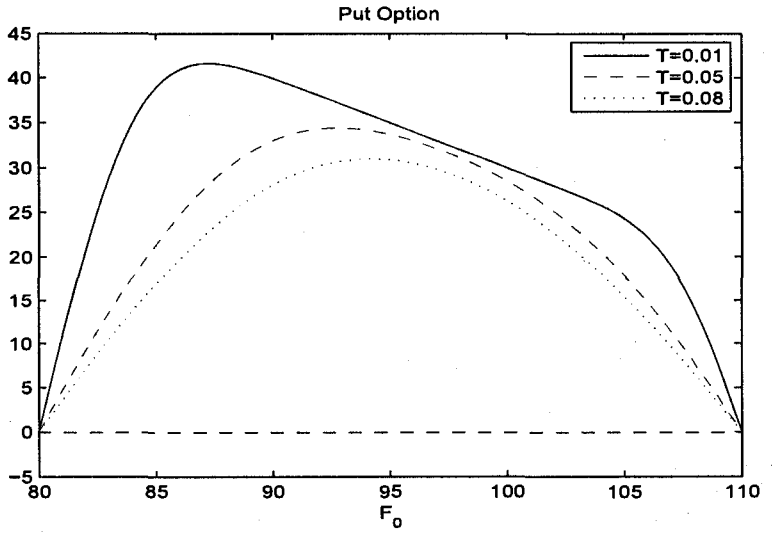


Figure 3.2.7: Converged double knock-out put values with various $T$.

The three individual curves correspond to the three separate sets of families depicted in Figure 2.3.1. The curve corresponding to the steepest local

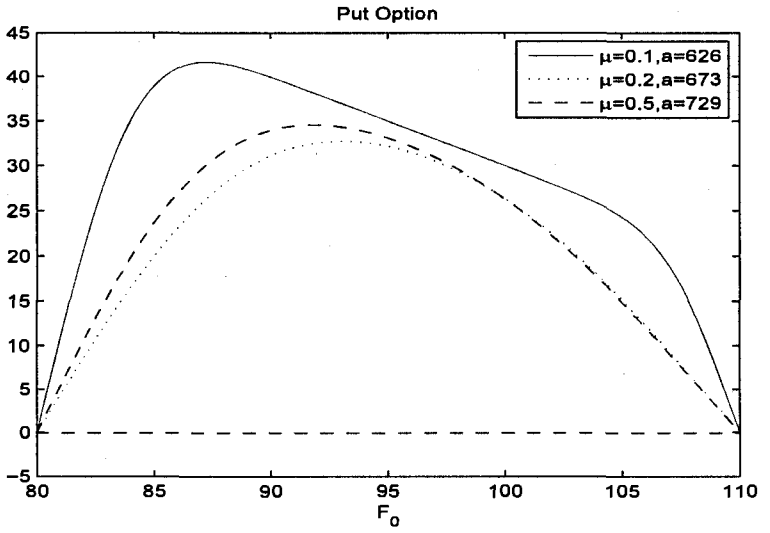


Figure 3.2.8: Converged double knock-out put with different choices of $(\mu, a)$.

volatility model ($\mu = 0.1$) displays a pronounced skewness in the double-barrier put option price as function of spot $F_0$.

**3.2.2. Up-and-Out Put.** Here we derive the up-and-out put option pricing formula, denoted by $P(H, F_0, K, T)$, where $H$ is an upper barrier. The derivations are similar to that of the up-and-out call. The derivation is based upon a limiting procedure where we take $L \to 0+$ within the double knock-out put option formula $P(L, H, F_0, K, T)$. The derivation given below takes into account the possibility of the asset price hitting zero (i.e. default) before maturity.

By risk-neutral pricing we have

$$\begin{aligned} P(H, F_0, K, T) &= e^{-rT}\mathbb{E}\left[\Lambda^{(H)}(\mathrm{F}_T)|\mathrm{F}_0 = F_0\right] \\ &= e^{-rT}\mathbb{E}\left[(K - \mathrm{F}_T)^+ \mathbb{1}_{\{\tau_0 > T, \tau_H > T\}}|\mathrm{F}_0 = F_0\right] \\ &+ Ke^{-rT}\mathbb{E}\left[\mathbb{1}_{\{\tau_0 \leq T, \tau_0 < \tau_H\}}|\mathrm{F}_0 = F_0\right] \end{aligned} \tag{3.2.6}$$

The second term corresponds to the discounted put payoff under scenarios where the asset price hits zero (i.e. default) before hitting the upper barrier level $H$, before maturity time $T$. The first expectation term is equivalent to

$$\lim_{L\to 0+} e^{-rT}\mathbb{E}\left[(K - \mathrm{F}_T)^+ \mathbb{1}_{\{\tau_L > T, \tau_H > T\}}|\mathrm{F}_0 = F_0\right] = \lim_{L\to 0+} P(L, H, F_0, K, T)$$

Hence, equation (3.2.6) becomes:

$$P(H, F_0, K, T) = \lim_{L\to 0+} P(L, H, F_0, K, T) + Ke^{-rT}\mathbb{E}\left[\mathbb{1}_{\{\tau_0 \leq T, \tau_0 < \tau_H\}}|\mathrm{F}_0 = F_0\right] \tag{3.2.7}$$

Using equation (2.2.6) then gives

$$P(H, F_0, K, T) = \lim_{L\to 0+} P(L, H, F_0, K, T) + Ke^{-rT} \lim_{L\to 0+} \mathbb{P}\{\tau_L^-(H) \leq T\} \tag{3.2.8}$$

where $\tau_L^-(H)$ is defined in equation (2.2.4) and $\mathbb{P}\{\tau_L^-(H) \leq T\}$ is the risk-neutral probability that the process $\mathrm{F}_t$ starts at $F_0 \in [L, H]$ and is absorbed at the lower level $L$ before it is killed at upper level $H$. The derivation of this probability is given by Campolieti 2008 and has the closed-form spectral expansion

$$\mathbb{P}\{\tau_L^-(H) \leq T\} = \Phi^-(\infty; F_0, L|H) - \mathbb{P}\{T < \tau_L^-(H) < \infty\} \tag{3.2.9}$$

where

$$\Phi^{-}(\infty; F_0, L|H) = \frac{R_\mu(\sqrt{2\rho x_H}) - R_\mu(\sqrt{2\rho x_0})}{R_\mu(\sqrt{2\rho x_H}) - R_\mu(\sqrt{2\rho x_L})} \tag{3.2.10}$$

$R_\mu(z) := I_\mu(z)/K_\mu(z)$ and

$$\mathbb{P}\{T < \tau_L^-(H) < \infty\} = \frac{K_\mu(\sqrt{2\rho x_L})}{K_\mu(\sqrt{2\rho x_0})} \sum_{n=1}^{\infty} \left(\frac{\mathcal{N}_n^2}{\pi}\right) \frac{e^{-(\rho+\lambda_n)T}}{(\rho+\lambda_n)} f_\mu(x_0, x_L, \lambda_n) \tag{3.2.11}$$

In equations (3.2.10) and (3.2.11), $x_L = \mathsf{X}(L)$, $x_H = \mathsf{X}(H)$ and $x_0 = \mathsf{X}(F_0)$ where $\mathsf{X} := \mathsf{F}^{-1}$ is the inverse map given by equation (2.3.3). $f_\mu(x, y, \lambda)$ and $\mathcal{N}_n$ are the Bessel cylinder function and the normalization constant, respectively, given in equation (1.2.6).

Finally, substituting (3.2.9) into (3.2.8) gives

$$\begin{aligned} P(H, F_0, K, T) = {} & Ke^{-rT} \lim_{L \to 0+} \left(\Phi^{-}(\infty; F_0, L|H) - \mathbb{P}\{T < \tau_L^-(H) < \infty\}\right) \\ & + e^{-rT} \lim_{L \to 0+} \left[K\Phi(\max\{H, K\}, F_0, T) - \overline{\Phi}(\max\{H, K\}, F_0, T)\right] \end{aligned} \tag{3.2.12}$$

where $\Phi$ and $\overline{\Phi}$ are given in equations (3.0.11) and (3.0.17), respectively.

Figure 3.2.9 shows the double-barrier put values $P(L, H, F_0, K, T)$ converge to $P(H, F_0, K, T)$ as $L \to 0+$, with $H = 110, \rho = 0.00001, \mu = 0.1, a = 626, r = 0.02, T = 0.1, K = 90$.

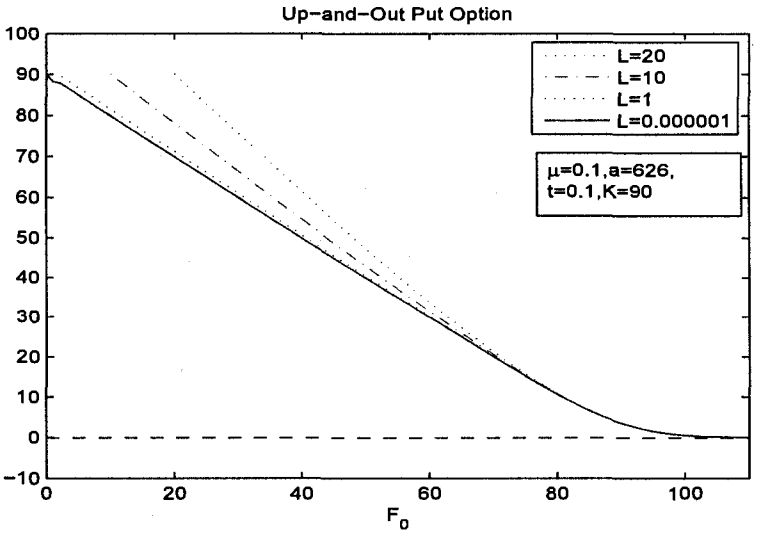


Figure 3.2.9: Convergence of up-and-out put value.

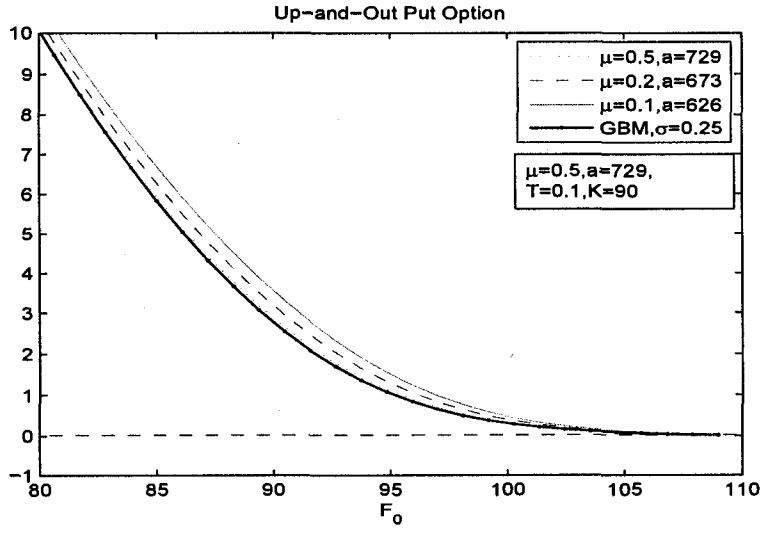


Figure 3.2.10: Converged up-and-out put value and GBM model.

Figure 3.2.10 displays the converged up-and-out put values for the drifted Bessel-$K$ model with three different sets of parameters $(\mu, a)$ and the up-and-out put value for the GBM model (solid dotted line), with local volatility $\sigma = 0.25 = \sigma(F_0)/F_0$ at $F_0 = 100$, where $H = 110, \rho = 0.00001, r = 0.02, T = 0.1, K = 90$. As seen, the three curves of $P(H, F_0, K, t)$ for the Bessel-$K$ diffusions give fairly different results. Especially for smaller values of spot $F_0 \lesssim 95$. The Bessel-$K$ model is closer to the GBM model for larger $\mu$ values. For smaller values of $\mu$ the local volatility curves are steeper and deviate drastically from the constant local volatility line of the GBM model.

## 3.3. Recovering CEV Models from Bessel K-Subfamily

In this section we recover the zero-drift CEV model, i.e. with asset price process $\mathrm{F}_t, t \geq 0$, obeying the SDE

$$d\mathrm{F}_t = \delta \mathrm{F}_t^{1+\beta} dW_t, \tag{3.3.1}$$

as a special limiting case of the zero-drift Bessel $K$-subfamily. The volatility function for the CEV model follows a power law where $\sigma(F) = \delta F^{1+\beta}$. Throughout we consider the case where $\delta > 0$, $\beta < 0$ which leads to a martingale diffusion. For the general connection between the CEV and the Bessel family of diffusions, we refer the reader to the papers by Campolieti and Makarov 2006. In this thesis we further establish the pricing kernels and consequently derive closed-form pricing formulas for barrier options for the driftless CEV diffusion with imposed killing at barriers. Following Campolieti and Makarov, the derivation is based upon setting the drift $\theta = 0$ and taking the limit $\rho \to 0+$, while keeping $a\rho^{\mu}$ constant along the limit, within the drifted Bessel-$K$ formulas, and using the small argument

asymptotic forms of the modified Bessel functions $I_\mu(z)$ and $K_\mu(z)$, with order $\mu > 0$.

Now, taking $\rho \to 0+$, with $\theta = 0$, within the map $F = \mathsf{F}(x)$ (for the Bessel $K$-subfamily defined in equation (2.3.3)), we have:

$$\begin{aligned}\mathsf{F}(x) &\approx a\frac{1}{\Gamma(\mu+1)}\left(\frac{\sqrt{2\rho x}}{2}\right)^{\mu}\frac{1}{(2/\sqrt{2\rho x})^{\mu}\Gamma(\mu)/2} \\ &\approx 2a(\rho/2)^{\mu}[\Gamma(\mu+1)\Gamma(\mu)]^{-1}x^{\mu} \\ &\to Cx^{\mu}\end{aligned} \tag{3.3.2}$$

where we define the constant $C = 2a(\rho/2)^{\mu}[\Gamma(\mu+1)\Gamma(\mu)]^{-1}$. $\Gamma(\cdot)$ is the standard gamma function. Moreover, we set $\mu = 1/(2|\beta|)$ ($\beta = -(2\mu)^{-1}$) and the above map reduces to

$$\mathsf{F}(x) \approx \left(\delta^2\beta^2 x\right)^{\frac{1}{2|\beta|}} \tag{3.3.3}$$

with inverse $\mathsf{X} := \mathsf{F}^{-1}$:

$$\mathsf{X}(F) = \frac{F^{2|\beta|}}{(\delta\beta)^2} = \frac{F^{-2\beta}}{\delta^2\beta^2} \tag{3.3.4}$$

Applying the above limiting procedure, the volatility function $\sigma(F)$ in (2.3.3) becomes

$$\begin{aligned}\sigma(F) &= \frac{a}{\sqrt{x}K_{\mu}^2(\sqrt{2\rho x})} \\ &\approx a\frac{1}{\sqrt{x}[\Gamma(\mu)/2(2/\sqrt{2\rho x})^{\mu}]^2}\end{aligned} \tag{3.3.5}$$

Now, substituting $a = \frac{\Gamma(\mu+1)\Gamma(\mu)}{2(\rho/2)^{\mu}}(\delta/2\mu)^{2\mu}$ and using $x = \mathsf{X}(F)$ into equation (3.3.5), along with the property $\Gamma(\mu+1)/\Gamma(\mu) = \mu = 1/2|\beta|$, leads (as

required) to the above CEV volatility:

$$\sigma(F) = \delta F^{1-|\beta|} = \delta F^{1+\beta} \tag{3.3.6}$$

Let $U^{CEV}(F, F_0, L, H, t)$ denote the double-barrier transition probability density of a zero-drift CEV model, with $L$ and $H$ as lower and upper barriers, respectively. An analytically exact spectral expansion for $U^{CEV}(F, F_0, L, H, t)$ is now obtained by applying the above limiting procedure to the transition density for the Bessel-$K$ process. That is, setting $\theta = 0$ and taking $\rho \to 0+$ within equation (2.4.1) gives

$$U^{CEV}(F, F_0, L, H, t) \to \frac{\sqrt{\mathsf{X}(F)}}{\sigma(F)} \left( \frac{\mathsf{X}(F)}{\mathsf{X}(F_0)} \right)^{-\mu} \sum_{n=1}^{\infty} e^{-\lambda_n t} \Upsilon(\mu, x, x_0, x_L, n) \tag{3.3.7}$$

where $\Upsilon(\mu, x, x_0, x_L, n) = \mathcal{N}_n^2 f_\mu(x_0, x_L, \lambda_n) f_\mu(x, x_L, \lambda_n)$. Using the mapping in (3.3.4) gives the explicit closed-form transition density

$$U^{CEV}(F, F_0, L, H, t) = \frac{\sqrt{F_0} F^{-2\beta-3/2}}{|\beta|\delta^2} \sum_{n=1}^{\infty} e^{-\lambda_n t} \mathcal{N}_n^2 f_\mu(x_0, x_L, \lambda_n) f_\mu(x, x_L, \lambda_n) \tag{3.3.8}$$

where $f_\mu$, $\mu = \frac{1}{2|\beta|}$, and $\mathcal{N}_n$ are the Bessel cylinder function and normalization given in equation (1.2.6) with values $x = \mathsf{X}(F) = \frac{F^{-2\beta}}{\delta^2\beta^2}$, $x_0 = \mathsf{X}(F_0) = \frac{F_0^{-2\beta}}{\delta^2\beta^2}$, $x_L = \mathsf{X}(L) = \frac{L^{-2\beta}}{\delta^2\beta^2}$, $x_H = \mathsf{X}(H) = \frac{H^{-2\beta}}{\delta^2\beta^2}$.

Figure 3.3.1 shows the rapidly convergent plots of the transition density $U^{CEV}(F, F_0, t)$ with fixed values $F_0 = 3, L = 2, H = 10, t = 10, \beta = -2, \delta = 2$. The five different curves correspond to the first $N = 2, 4, 8, 12$ and 20 terms of the series in equation (3.3.8).

Figure 3.3.2 gives converged plots of the series in equation (3.3.8) with different values of time $t$, where $F_0 = 3, L = 2, H = 10, \beta = -2, \delta = 2$.

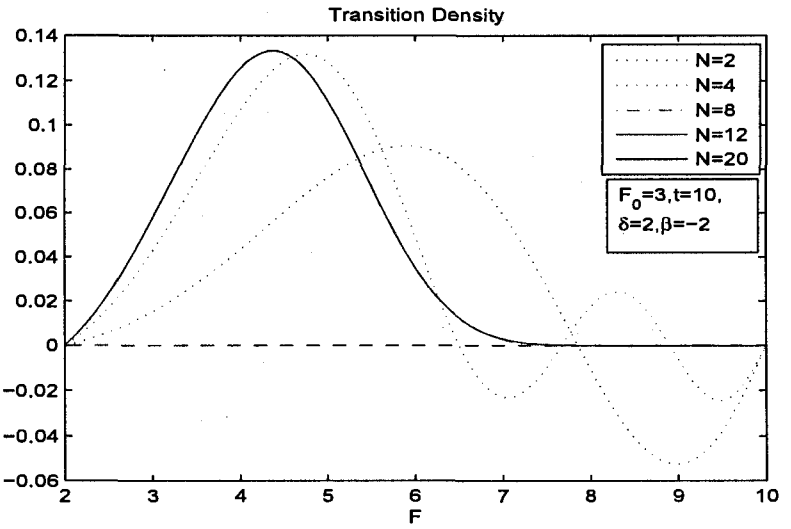


Figure 3.3.1: Convergence of CEV transition density.

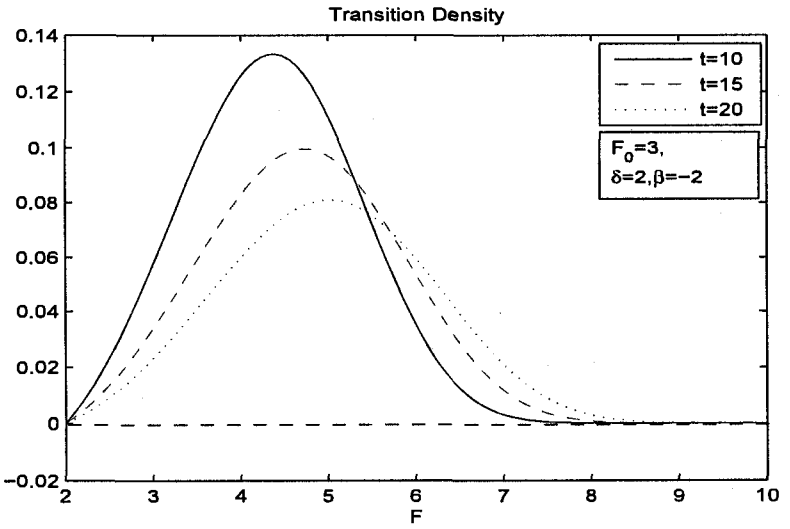


Figure 3.3.2: Converged CEV density with various $t$.

The exact spectral expansion for the cumulative transition density of the CEV volatility model, $\Phi^{CEV}(F, F_0, t) := \int_L^F U^{CEV}(\overline{F}, F_0, L, H, t)d\overline{F}$, is

readily obtained by the above limit approach. That is, setting $\theta = 0$ and taking $\rho \to 0+$, while using the asymptotic form $K_\mu(z) \sim \frac{1}{2}\Gamma(\mu)(\frac{z}{2})^{-\mu}$, gives

$$\Phi^{CEV}(F, F_0, t) = \lim_{\rho \to 0+} \frac{x_0^{\mu/2}(\rho/2)^{\mu/2}}{\Gamma(\mu)} \sum_{n=1}^{\infty} e^{-\lambda_n t} \mathcal{N}_n f_\mu(x_0, x_L, \lambda_n) \Psi_{n,\rho}(x) \tag{3.3.9}$$

As $\rho \to 0+$, $\Psi_{n,\rho}(x)$ in equation (3.0.14) has the leading asymptotic form

$$\Psi_{n,\rho}(x) \sim \frac{\Gamma(\mu)\,(\rho/2)^{-\mu/2}}{\lambda_n} \left[ -\sqrt{\frac{\lambda_n}{2}} x^{1/2-\mu/2} \widetilde{\phi}_n(x) - \mu \phi_n(x) + \frac{2}{\pi} \mathcal{N}_n x_L^{-\mu/2} \right] \tag{3.3.10}$$

Hence, using this latter asymptotic form into equation (3.3.9) gives us the exact spectral expansion for $\Phi^{CEV}(F, F_0, t)$:

$$\begin{aligned} \Phi^{CEV}(F, F_0, t) &= x_0^{\mu/2} \sum_{n=1}^{\infty} \frac{e^{-\lambda_n t}}{\lambda_n} \mathcal{N}_n f_\mu(x_0, x_L, \lambda_n) \\ &\times \left[ -\sqrt{\frac{\lambda_n}{2}} x^{1/2-\mu/2} \widetilde{\phi}_n(x) - \mu \phi_n(x) + \frac{2}{\pi} \mathcal{N}_n x_L^{-\mu/2} \right] \end{aligned} \tag{3.3.11}$$

Similarly, $\overline{\Phi}^{CEV}(F, F_0, t) := \int_L^F U^{CEV}(\overline{F}, F_0, L, H, t) \overline{F} d\overline{F}$, is obtained by applying the above limit to the expressions in equations (3.0.17), (3.0.20) with drift $r = 0$ and simplifying. The related cumulative distribution has the closed-form spectral expansion:

$$\begin{aligned} \overline{\Phi}^{CEV}(F, F_0, t) &= \frac{1}{2} \left(\frac{\delta}{2\mu}\right)^{2\mu} x_0^{\mu/2} \sum_{n=1}^{\infty} \frac{e^{-\lambda_n t}}{\lambda_n} \mathcal{N}_n f_\mu(x_0, x_L, \lambda_n) \\ &\times \left[ -\sqrt{2\lambda_n} x^{1/2+\mu/2} \widetilde{\phi}_n(x) + \frac{2}{\pi} \mathcal{N}_n x_L^{\mu/2} \right] \end{aligned} \tag{3.3.12}$$

In both equations (3.3.11) and (3.3.12): $\mu = \frac{1}{2|\beta|}$, $x = \frac{F^{-2\beta}}{\delta^2\beta^2}$, $x_0 = \frac{F_0^{-2\beta}}{\delta^2\beta^2}$, $x_L = \frac{L^{-2\beta}}{\delta^2\beta^2}$, $x_H = \frac{H^{-2\beta}}{\delta^2\beta^2}$, with $\widetilde{\phi}_n(x)$ and $\phi_n(x)$ given by equations (3.0.15) and (1.2.5)-(1.2.6), respectively, with eigenvalues solving equation (1.2.7).

**3.3.1. Pricing Formulas for Zero-Drift CEV.** In this subsection, we develop the analytical double-knock-out European call and put pricing formulas for the zero-drift CEV volatility model. Let $C^{CEV}(F_0, K, T)$ denote the double-knock-out call option value with lower barrier $L$ and upper barrier $H$, with payoff $\Lambda^{(L,H)}$ given in equation (3.0.5). Since we are dealing with the zero-drift case, then asset prices are driftless under the assumed risk-neutral measure $\mathbb{P}$. Hence, in what follows we are pricing options under the CEV model with the assumption of zero (negligible) interest rate with $(\mathrm{F}_t)_{t\geq 0}$ representing the asset (e.g. stock) price process.

For the case where $L \leq K \leq H$ we have

$$\begin{aligned} C^{CEV}(F_0, K, T) &= \mathbb{E}\left[(\mathrm{F}_T - K)^+ \mathbb{1}_{\{\tau_H > T, \tau_L > T\}} | \mathrm{F}_0 = F_0\right] \\ &= \int_L^H U(F, F_0, L, H, T)(F - K)^+ dF \\ &= \overline{\Phi}^{CEV}(H, F_0, T) - \overline{\Phi}^{CEV}(K, F_0, T) \\ &\quad - K\left[\Phi^{CEV}(H, F_0, T) - \Phi^{CEV}(K, F_0, T)\right] \end{aligned} \tag{3.3.13}$$

where $\Phi^{CEV}$ and $\overline{\Phi}^{CEV}$ are given by equations (3.3.11) and (3.3.12), respectively.

Figure 3.3.3 gives plots for the computed double-knock-out call using equation (3.3.13) as function of spot $F_0$, where $F_0 = 3, L = 2, H = 10, T = 10, \beta = -2, \delta = 2, K = 5$. As shown, $C^{CEV}(F_0, K, T)$ converges rapidly as more terms are added to the series. The five curves correspond to the first $N = 2, 4, 8, 12$ and 20 terms of the series sums in equations (3.3.11) and (3.3.12).

Figure 3.3.4 shows converged plots for $C^{CEV}(F_0, K, T)$ with fixed $F_0 = 3, L = 2, H = 10, T = 10, \beta = -2, \delta = 2$ and various choices of strike $K$.

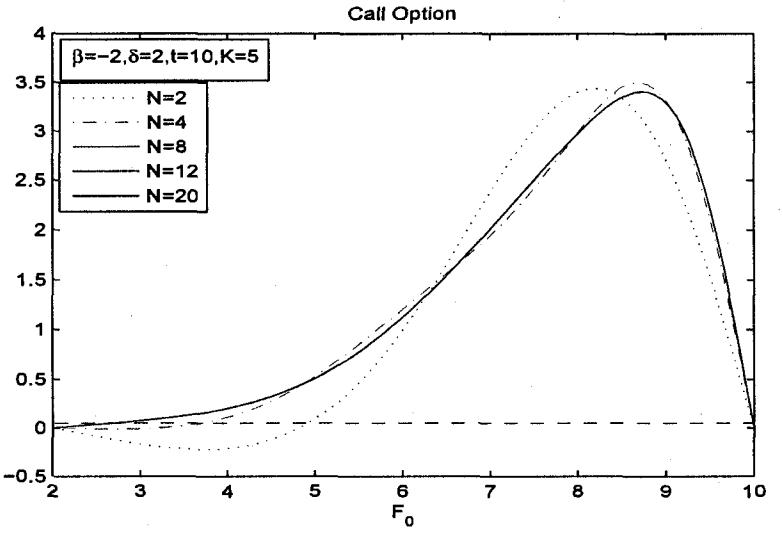


Figure 3.3.3: Convergence of double knock-out call series for CEV model.

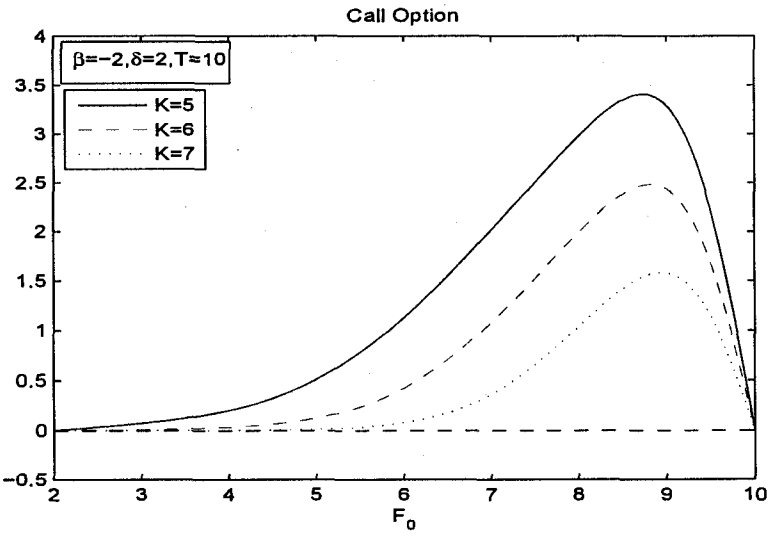


Figure 3.3.4: Converged double knock-out European call value CEV model.

Figure 3.3.5 demonstrates the converged plots of the double-knock-out call using equation (3.3.13), with different choices of $T$ and fixed $F_0 = 3, L = 2, H = 10, \beta = -2, \delta = 2, K = 5$.

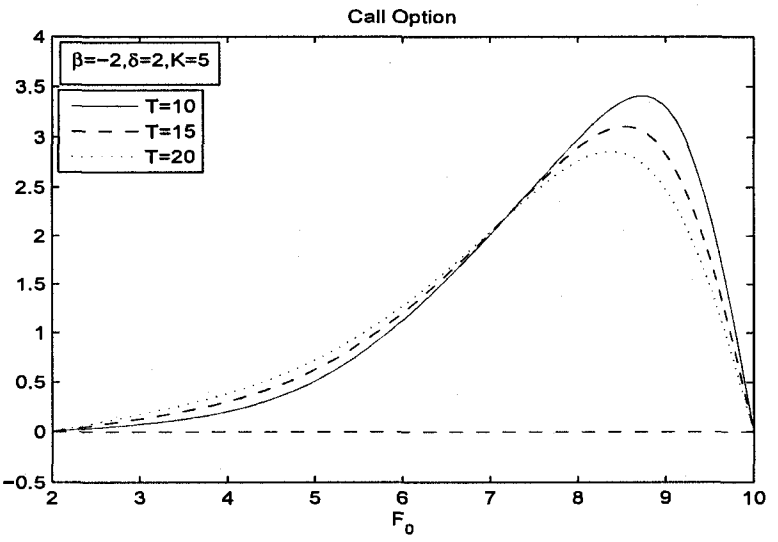


Figure 3.3.5: Converged double-knock-out CEV model with various maturities.

Similarly, for strike price $K$ below the barriers (ie $K \leq L \leq H$), we have:

$$\begin{aligned} C^{CEV}(F_0, K, T) &= \int_L^H U^{CEV}(F, F_0, L, H, T)(F-K)^+ dF \\ &= \overline{\Phi}^{CEV}(H, F_0, T) - K\Phi^{CEV}(H, F_0, T) \end{aligned} \tag{3.3.14}$$

Figure (3.3.6) presents some converged plots of equation (3.3.14) with fixed parameters $F_0 = 3, L = 2, H = 10, T = 10, \beta = -2, \delta = 2$. The three distinct graphs correspond to the three different strike prices $K$. Figure(3.3.7) gives plots for $C^{CEV}(F_0, K, T)$ as function of spot $F_0$ with $F_0 = 3, L = 2, H = 10, T = 10, \beta = -2, \delta = 2$ and various times $T$.

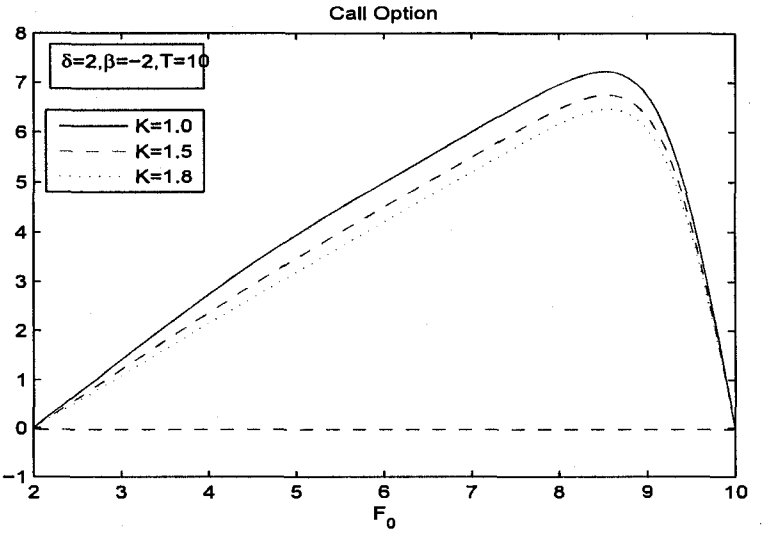


Figure 3.3.6: double knock-out call CEV model with $K \leq L \leq H$.

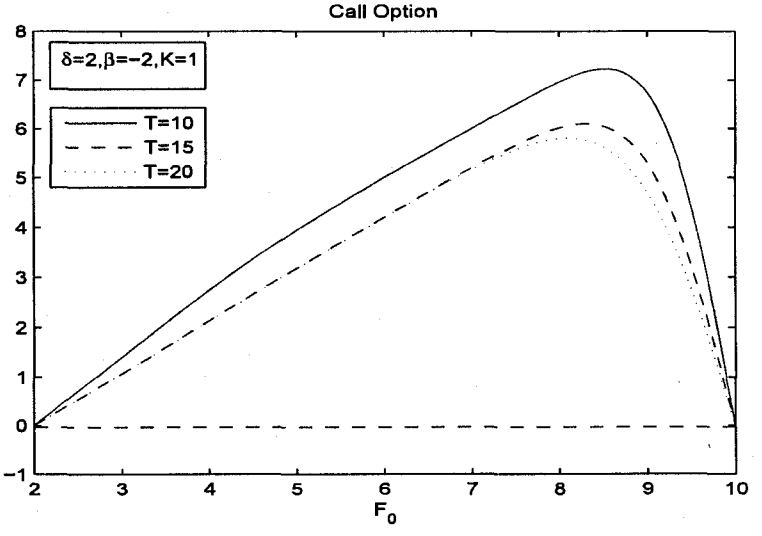


Figure 3.3.7: Double-knock-out call for CEV model with various $T$ values.

The double-knock-out put pricing formula for the zero-drift CEV model, denoted by $P^{CEV}(L, H, F_0, K, t)$, is derived as follows. For $L \leq K \leq H$,

$$\begin{aligned} P^{CEV}(L, H, F_0, K, T) &= \mathbb{E}\left[(K - F_T)^+ \mathbb{1}_{\{\tau_H > T, \tau_L > T\}} | \mathrm{F}_0 = F_0\right] \\ &= \int_L^H U^{CEV}(F, F_0, L, H, T)(K - F)^+ dF \quad (3.3.15) \\ &= K\Phi^{CEV}(K, F_0, T) - \overline{\Phi}^{CEV}(K, F_0, T) \end{aligned}$$

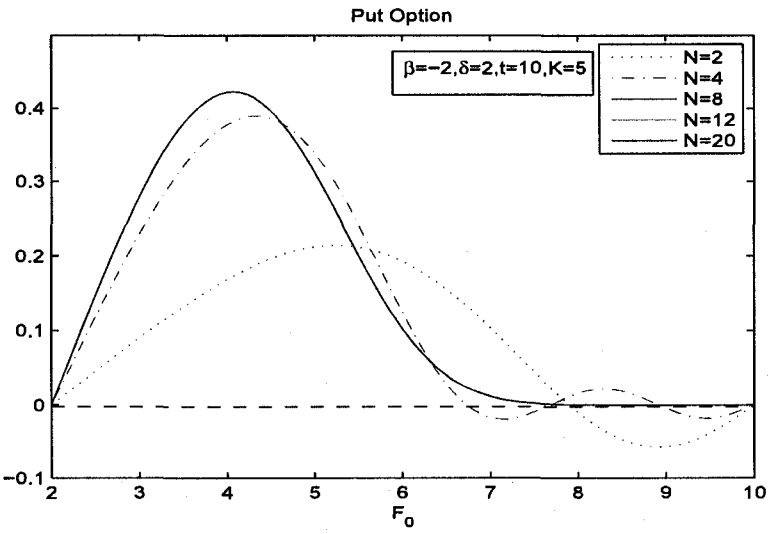


Figure 3.3.8: Rapidly convergent double-knock-out put series for CEV model.

Figure (3.3.8) shows rapidly convergent plots for the series of equation $P^{CEV}(L, H, F_0, K, T)$ with fixed parameters $F_0 = 3, L = 2, H = 10, T = 10, \beta = -2, \delta = 2, K = 5$. The five graphs represent the first $N = 2, 4, 8, 12$ and 20 (solid line) terms of the series sum of equation (3.3.15).

Figure (3.3.9) gives converged plots of equation (3.3.15) with different strike price $K$ and fixed parameters $F_0 = 3, L = 2, H = 10, T = 10, \beta = -2, \delta = 2$.

Figure (3.3.10) provides the converged plots of $P^{CEV}(L, H, F_0, K, T)$ with different values of $T$ and fixed parameters $F_0 = 3, L = 2, H = 10, K = 5, \beta = -2, \delta = 2$.

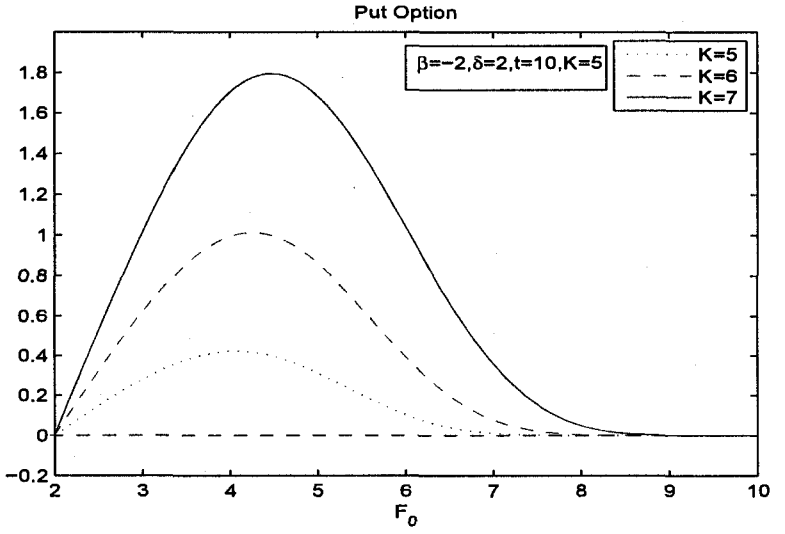


Figure 3.3.9: Converged double-knock-out put for CEV model with various $K$.

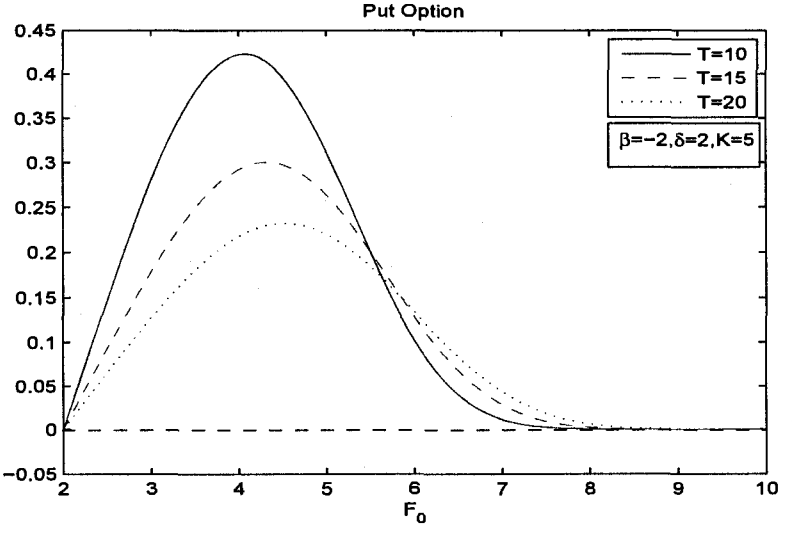


Figure 3.3.10: Converged double-knock-out put values with various $T$.

Similarly, for the case where $L \leq H \leq K$, we have:

$$\begin{aligned} P^{CEV}(L,H,F_0,K,T) &= \mathbb{E}\left[(K-F_T)^+ \mathbb{1}_{\{\tau_H>T,\tau_L>T\}} | \mathrm{F}_0 = F_0\right] \\ &= \int_L^H U^{CEV}(F,F_0,L,H,T)(K-F)^+ dF \quad (3.3.16) \\ &= K\Phi^{CEV}(H,F_0,T) - \overline{\Phi}^{CEV}(H,F_0,T) \end{aligned}$$

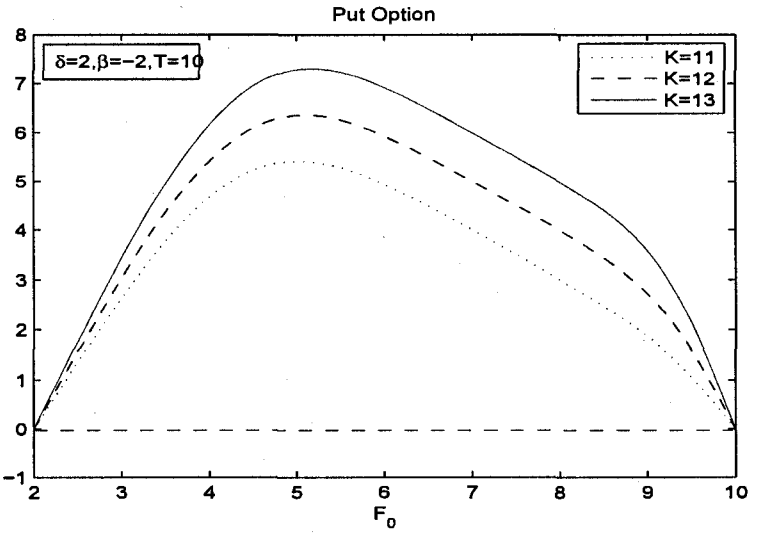


Figure 3.3.11: Double-knock-out put for CEV model with $L \leq H \leq K$.

Figure (3.3.11) displays the converged plots of equation (3.3.16) with different strike price $K$ and fixed parameters $F_0 = 3, L = 2, H = 10, T(= t) = 10, \beta = -2, \delta = 2$.

Figure (3.3.12) gives plots of the double knock-out put value $P^{CEV}(L, H, F_0, K, T)$, computed using the series in equation (3.3.16) where $L \leq H \leq K$. The three distinct curves represent the three different times to maturity $T$ with fixed parameters $F_0 = 3, L = 2, H = 10, K = 5, \beta = -2, \delta = 2$.

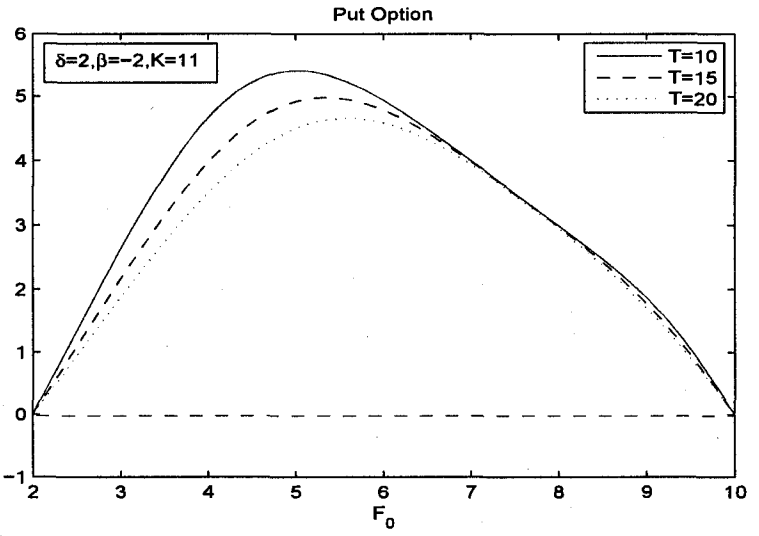


Figure 3.3.12: Convergence of double knock-out put for CEV model with various $T$.

CHAPTER 4

# Sensitivity Analysis For European Barrier Call Option

In this chapter, we present a sensitivity analysis of the double knock-out European call options under the new family of drifted Bessel-$K$ diffusion models. That is, in financial terminology we study the so-called "Greeks" associated to the barrier options. The name Greeks is used because it is standard notation to denote certain derivatives of an option value by particular Greek letters. The derivatives represent the sensitivities of a given option value under changes in an underlying parameter or asset price. In this thesis we shall only focus on the explicit analysis of the knock-out call. In particular, the double knock-out call price $C(L, H, F_0, K, T)$ is given by equation (3.1.3), in Section 3.1.1. Its value can be re-written in a more convenient form, i.e.

$$C(L, H, F_0, K, T) = \frac{e^{-rT}}{2K_\mu(\sqrt{2\rho x_0})} \sum_{n=1}^{\infty} e^{-(\rho+\lambda_n)T} \mathcal{N}_n \Omega_{n,\rho} f_\mu(x_0, x_L, \lambda_n) \tag{4.0.17}$$

where

$$\Omega_{n,\rho} = a\left[\overline{\Psi}_{n,\rho}(x_H) - \overline{\Psi}_{n,\rho}(x_K)\right] - K\left[\Psi_{n,\rho}(x_H) - \Psi_{n,\rho}(x_K)\right] \tag{4.0.18}$$

$f_\mu(x_0, x_L, \lambda_n)$ and $\mathcal{N}_n$ are defined in equation (1.2.6). $\Psi_{n,\rho}$, $\overline{\Psi}_{n,\rho}$ and $\widetilde{\phi}_n$ are given in equations (3.0.14), (3.0.15) and (3.0.20), respectively, and $x = \mathsf{X}(F), x_L = \mathsf{X}(L), x_H = \mathsf{X}(H)$, $x_K = \mathsf{X}(K)$ and $x_0 = \mathsf{X}(F_0)$ are the unique inverse maps $\mathsf{X} := \mathsf{F}^{-1}$ in equation (2.3.3).

## 4.1. Delta

Here, we derive the so-called Delta, denoted by $\Delta$, of the European double knock-out call option. $\Delta$ measures the change in the option value due to small changes in the underlying asset price. The delta is of primary importance in hedging risk for portfolios of options. $\Delta$ is defined as the first derivative of $C(L, H, F_0, K, T)$ (in this case) with respect to the spot price $F_0$, i.e.

$$\Delta = \frac{\partial C}{\partial F_0} \tag{4.1.1}$$

Now, using $|\mathsf{X}'(F_0)| = 2\sqrt{\mathsf{X}(F_0)}/\sigma(F_0)$, and the chain rule for differentiation, along with the Bessel recurrence relations, $J'_\mu(z) = \frac{\mu}{z}J_\mu(z) - J_{\mu+1}(z)$, $Y'_\mu(z) = \frac{\mu}{z}Y_\mu(z) - Y_{\mu+1}(z)$, $I'_\mu(z) = \frac{\mu}{z}I_\mu(z) + I_{\mu+1}(z), K'_\mu(z) = \frac{\mu}{z}K_\mu(z) + K_{\mu+1}(z)$, we obtain a closed-form spectral expansion

$$\Delta = \frac{e^{-rT}}{\sqrt{2}\sigma(F_0)K_\mu^2(\sqrt{2\rho x_0})} \sum_{n=1}^{\infty} e^{-(\rho+\lambda_n)T}\mathcal{N}_n\chi_{n,\rho}(x_0, x_L)\Omega_{n,\rho} \tag{4.1.2}$$

where $\sigma(F_0)$ is given by equation (2.3.3) and

$$\Omega_{n,\rho} = a\left[\overline{\Psi}_{n,\rho}(x_H) - \overline{\Psi}_{n,\rho}(x_K)\right] - K\left[\Psi_{n,\rho}(x_H) - \Psi_{n,\rho}(x_K)\right] \tag{4.1.3}$$

and

$$\chi_{n,\rho}(x_0, x_L) = \left[\frac{\sqrt{\lambda_n}}{\mathcal{N}_n}K_\mu(\sqrt{2\rho x_0})\widetilde{\phi}_n(x_0) + \sqrt{\rho}K_{\mu+1}(\sqrt{2\rho x_0})f_\mu(x_0, x_L, \lambda_n)\right]$$

The Delta of a single-barrier call can be computed by the previous limiting approach. That is, taking the limit $L \to 0^+$ of the double-barrier call $\Delta$ leads to the upper single-barrier call $\Delta$. Similarly, taking $H \to \infty$ gives the lower single-barrier call Delta. Some calculations for typical graphs of Delta as function of spot price are given below.

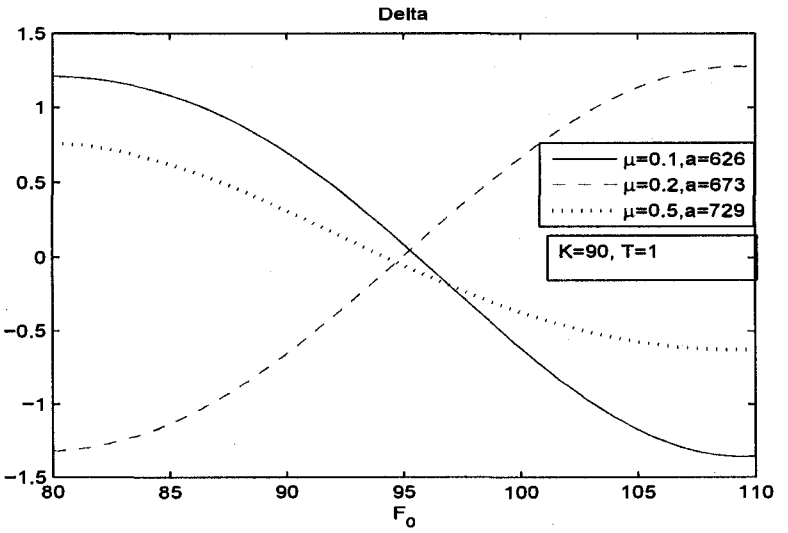


Figure 4.1.1: Double-knock-out call Delta values.

Figure 4.1.1 presents graphs of the double knock-out call Delta as function of spot using equation (4.1.2), with fixed parameters $L = 80, H = 110, K = 90, T = 1, \rho = 0.00001, r = 0.02$. The three distinct curves correspond to the three different families of Bessel-$K$ diffusion models (with different sets of values for parameters $(\mu, a)$).

Figure 4.1.2 gives the convergence plots of the down-and-out call Delta. The calculations were done by taking limit $L \to 0^+$ of the $\Delta$ defined in equation (4.1.2). The three curves represent the different sets of values $(\mu, a)$ within the different families of Bessel-$K$ diffusion models, with fixed parameters $L = 80, H = 110, K = 90, T = 1, \rho = 0.00001$.

We observe that the values $(\mu, a)$ have a dramatic effect on both the double knock-out and up-and-out call Delta values of the Bessel-$K$ model, as seen in Figures 4.1.1 and 4.1.2, respectively. This is also observed in Davydov and Linetsky, 2001. In their CEV model, the parameter $\beta$ has

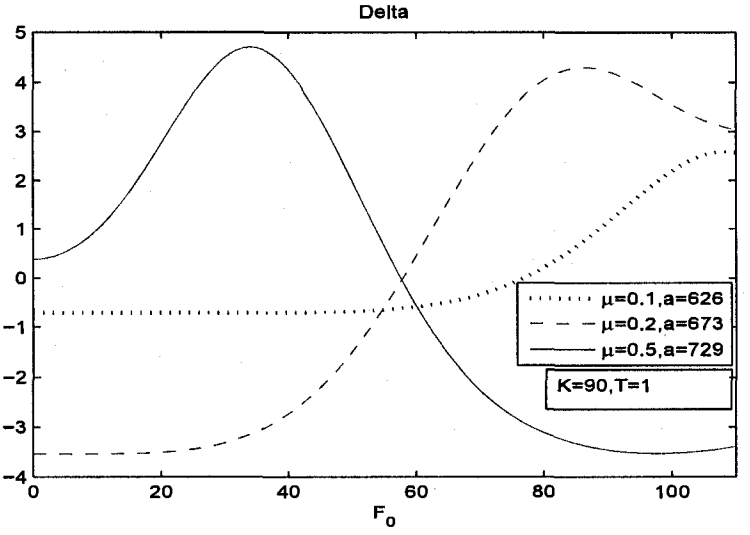


Figure 4.1.2: Converged up-and-out call Delta curve.

a similar effect on the CEV double knock-out and up-and-out call Delta values.

## 4.2. Theta

Here we compute the knock-out call Theta value, denoted by $\Theta$. $\Theta$ is given by the first derivative of the option value with respect to the time to expiration $T$. It hence measures the rate of change of the option value with respect to maturity. In other words, $\Theta$ represents the time decay on the value of the option.

Using $C(L, H, F_0, K, T)$ given in equation (4.0.17), and differentiating the series with respect to $T$ trivially gives

$$\begin{aligned}\Theta &= \frac{\partial}{\partial T} C(L, H, F_0, K, T) \\ &= \frac{-e^{-rT}}{2K_\mu(\sqrt{2\rho x_0})} \sum_{n=1}^{\infty} (\rho + r + \lambda_n) e^{-(\rho+\lambda_n)T} \mathcal{N}_n \Omega_{n,\rho} f_\mu(x_0, x_L, \lambda_n)\end{aligned} \tag{4.2.1}$$

The single-barrier call $\Theta$ value is then obtained via a similar limiting procedure as above. That is, by taking $L \to 0^+$ within the double-barrier Theta we obtain the upper single-barrier call Theta and taking $H \to \infty$ gives the lower single-barrier Theta.

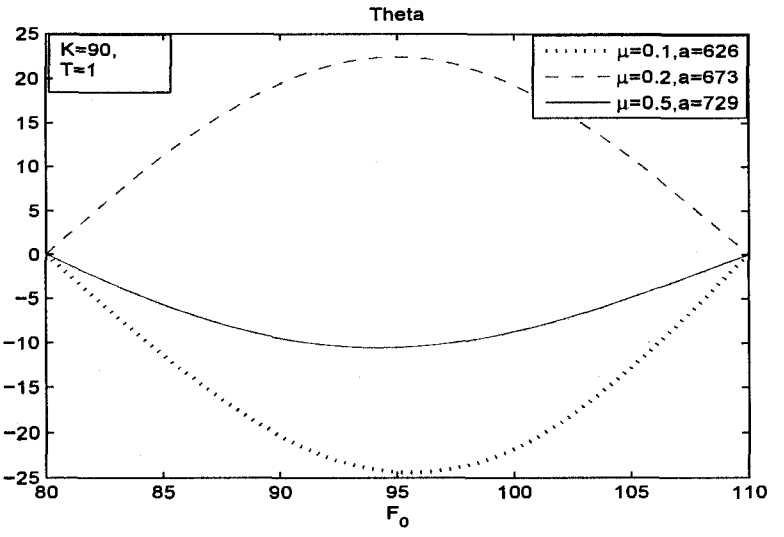


Figure 4.2.1: Double-knock-out call Theta values.

Figure 4.2.1 shows plots of the double-knock-out call Theta using equation (4.2.1), as function spot $F_0$, with $L = 80, H = 110, K = 90, T = 1, \rho = 0.00001, r = 0.02$. The three different graphs represent the three distinct families of Bessel-$K$ (i.e. with different sets of values $(\mu, a)$).

Figure 4.2.2 presents the converged up-and-out Theta curves as the limit $L \to 0^+$ of the down-and-out call Theta. The three curves represent the convergence of the three families of drifted Bessel-$K$ (i.e. different choices of values $(\mu, a)$) with fixed parameters $L = 80, H = 110, K = 90, T = 1, \rho = 0.00001, r = 0.02$.

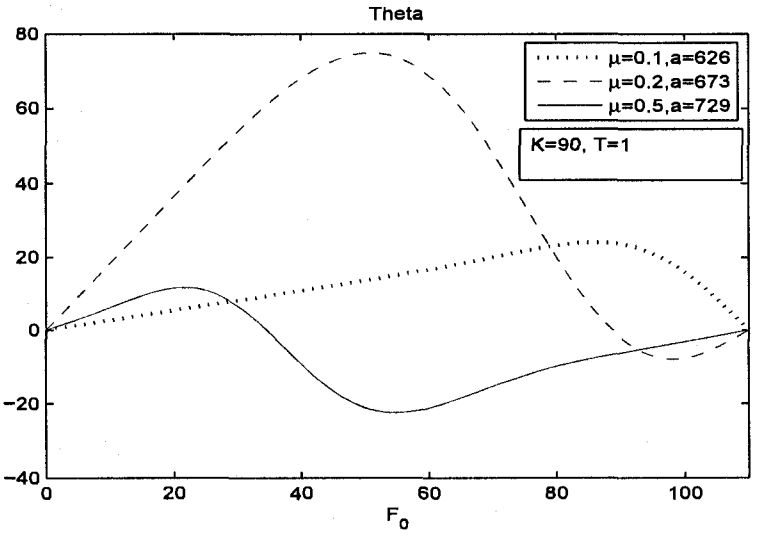


Figure 4.2.2: Converged up-and-out call Theta values.

In this chapter we have given only a brief account of the sensitivity analysis, namely of $\Delta$ and $\Theta$, for knock-out barrier options within the drifted Bessel-$K$ family of models. The other standard Greeks, i.e. such as the so-called Gamma ($\Gamma$), Vega ($\nu$) and Rho ($\rho$), are also readily computed via analogous closed-form spectral expansions and are left for future work.

# Conclusion and Future Work

In this thesis we developed analytically closed-form spectral expansions for pricing barrier options under new families of diffusion models (i.e. F-diffusions). The asset pricing models, referred to as the drifted Bessel family, are characterized by multi-parameter nonlinear local volatility functions. Our theoretical development made use of the so-called diffusion canonical transformation methodology. Particularly, we focussed on a four-parameter drifted Bessel $K$-subfamily. By applying the diffusion canonical transformation method with a combination of Green's function methods and first hitting time techniques, we arrived at new closed-from spectral expansions for barrier option pricing formulas as well as the corresponding sensitivities (Greeks).

We showed that the rapidly convergent spectral expansions are readily and efficiently implementable. The spectral expansions were derived in closed-form for killing at two barriers (i.e. double-barrier case) where the spectrum is simple and discrete. However, we also showed that by taking appropriate limits in one of the barrier levels, the double-barrier formulas lead to the single-barrier formulas. Our closed-form spectral expansions paved the way for efficiently carrying out various calculations of barrier options under the drifted Bessel $K$-subfamily for various choices of model parameters. Furthermore, we compared the results (for down-and-out and up-and-out call options, up-and-out put options) with the standard GBM

model. The deviation from the GBM model is very significant and the variability of this deviation can be modified with the choice of model parameters. In addition, we showed that by setting the drift parameter to zero and taking a particular limit, the four-parameter Bessel $K$-subfamily recovers the familiar zero-drift CEV local volatility model.

In the last chapter we presented closed-form spectral expansions for the Greeks associated to the barrier options under the new family of four-parameter drifted Bessel $K$ models. Although the sensitivity analysis that was presented is preliminary, the formalism is very useful for more thorough future studies. In particular, in future work the drifted Bessel-$K$ model can be calibrated to optimally fit a given implied volatility surface based on standard European call option market prices. Once the model parameters are calibrated, the closed-form spectral expansions provided in this thesis can be implemented to readily study the option prices as well as any of the "Greeks" for the barrier options.

Lastly, we remark that within this thesis the diffusion canonical transformation methodolgy and spectral expansion approaches were used to develop closed-form formulas for some barrier options, and their sensitivities, under the Bessel family. In fact we showed that such a family resulted as a consequence of considering the squared Bessel diffusion process as the solvable underlying model. This family is only one example among other families of so-called F-diffusions that are exactly solvable. The method presented in this thesis extends more generally to other solvable families of F-diffusions that have wide applicability in finance. Such families arise by considering other choices as the underlying solvable X-diffusion. For example, these include the Ornstein-Uhlenbeck process as well as the so-called confluent

hypergeometric family of processes. Further development and applications of these new models are the subject of future work.

# Bibliography


[1] G. Campolieti, Closed-form Spectral Expansions for New Families of Diffusion in Finance: First Hitting Time Densities and Lookback Option Pricing, submitted.

[2] C. Albanese and G. Campolieti, *Advanced Derivatives Pricing and Risk Management: Theory , Tools, and Hand-on Programming Applications.* Elsevier Academic Press 2005.

[3] D. Davydov and V. Linetsky, The Valuation and Hedging of Barrier and Lookback Option under the CEV Process, Management Science, 47, 949-965 (2001).

[4] V. Linetsky, Lookback Options and Diffusion Hitting Times: A Spectral Expansion Approach, Finance and Stochastics, 8, 373-398 (2004).

[5] G Campolieti and R Makarov, New Families of Solvable Affine Diffusion Models, 2008, Submitted to Stochastic Processes and Their Applications.

[6] G Camplieti and R Makarov (2006): On Properties of Analytically Solvable Families of Local Volatility Diffuson Models, to appear in Mathematical Finance.

[7] H. Taylor and S. Karlin, An Introduction to Stochastic Modelling.

[8] http://en.wikipedia.org/wiki/Greeks_(finance)

[9] http://en.wikipedia.org/wiki/Barrier_option

[10] Abramowitz M. and I.A. Stegum (1972): *Handbook of Mathematical Functions.* New York: Dover.

[11] Borodin A.N. and P. Salminen (2002): *Handbook of Brownian Motion-Facts and Formulae.* Springer.

[12] Cox J.C. (1975): "Notes on Option Pricing I: Constant Elasticity of Variance Diffusions." *Working paper*. Stanford University. Reprinted in *Journal of Portfolio Management*, 22 (1996), 15-17.

[13] Karlin S. and H.E. Taylor (1981): A second Course in Stochastic Processes. Academic Press.

[14] V. Linetsky (2004): The Spectral Decomposition Of the Option Value. *International Journal of Theoretical and Applied Finance*, 7, 337-384.

[15] Mandl P. (1968): Analytical Treatment of One-Dimensional Markov Processes. New York : Springer-Verlag.

[16] Rogers L.C.G. and D. Williams (2000): Diffusions, Markov Processes and Martingales, (Cambridge Mathematical Library). Cambridge University Press.

[17] Steven E. Shreve (2004): Stochastic Calculus for Finance II, Continuous-Time Model. Springer.